Structural and dielectric studies of ferroelectric Nd₂Ti₂O₇ for high temperature pyro sensor application

Bidesh Mahata

(MS17MTECH11009)

A Dissertation Submitted to

Indian Institute of Technology Hyderabad

In Partial Fulfillment of the Requirements for

The Degree of Master of Technology

भारतीय प्रौद्योगिकी संस्थान हैदराबाद

Indian Institute of Technology Hyderabad

Department of Materials Science & Metallurgical Engineering

June, 2019

Declaration

I declare that this thesis submission illustrates my own thoughts in my own words, and also others' concepts or words have been comprised, I have adequately cited and referenced the original sources. I also announce that I have adhered to all principles of academic honesty and integrity and have not misrepresented or falsified any idea/data/fact/source in my submission. I know that any violation of the above will be a reason to take disciplinary action by the Institute and can also evoke penal action from the sources that I have not been cited properly, or from whom proper consent has not been taken when needed.
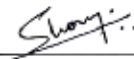
Bidesh Mahata.

—————————————————

(Signature)

BIDESH MAHATA

(MS17MTECH11009)

Approval Sheet

This thesis entitled "studies on electrical and structural stability of $Nd_2Ti_2O_7$ material for high temperature pyro sensor applications" by Bidesh Mahata is approved for the degree of Master of Technology from IIT Hyderabad.

Dr. Shourya Dutta Gupta
Assistant Professor
Department of Materials Science and Metallurgical Engineering
Examiner

Dr. Chandrasekhar Murapaka
Assistant Professor
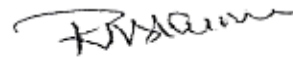Department of Materials Science and Metallurgical Engineering
Examiner

Dr. Ranjith Ramadurai
Associate Professor
Department of Materials Science and Metallurgical Engineering
Adviser

Dr. Sai Santosh Kumar Raavi
Associate Professor
Department of Physics
Chairman

iii

Acknowledgements

Dedicated to
IITH

Structural and dielectric studies of ferroelectric $Nd_2Ti_2O_7$ for high temperature pyro sensor application

Abstract

High temperature pyroelectric sensing technology is important in materials processing as well as in automotive and aerospace engineering. In aerospace it can be used as Exhaust Gas Temperature Sensor (EGTS) for hot chamber of jet engine as EGTS measures engine's health and other sensing application. The primary requirement from the material perspective is it must be stable in high temperature range (600 to 1000° C). Ferroelectric material with high T_c (>1000°C) can be used in temperature sensing technology due to its pyroelectric properties. Neodymium Titanate ($Nd_2Ti_2O_7$) is a promising candidate for this application as it has curie temperature of ~ 1480°C. NTO is a member of layered perovskite ferroelectric material. High T_c of NTO is due to the presence of dominant 180° ferroelectric domains and ferroelectric to paraelectric phase transition contains displacement of the whole sub lattice of TiO_6 octahedron.

In this thesis, we report the studies on synthesis of material, FullProf refinement and high temperature dielectric and pyroelectric properties of Neodymium Titanate material. Synthesis of NTO material is done by solid state reaction method. Neodymium oxide and titanium oxide is taken as primary materials in 1:2 molar ratios and the mixture is grinded with mortar and pestle for 4 hours. Phase purity is obtained by calcination of powder sample at 1250°C for 4 hours. XRD studies confirm the phase purity of neodymium titanate material. After ball milling powder is pressed to make pellet. Green pellets were sintered at 1400°C for 5 hours with a heating and cooling rates of 5°C/min. Detailed study of structural refinement was carried out by FullProf Suite software with CIF file taken from COD data base. SEM images of pellet shows densely packing of particles. Finally, dielectric property study is done by impedance analyzer instrument and furnace that goes up to 800°C. First experiment is done with applied voltage 0.8 V and data is taken during cooling from 750°C-50°C which shows the variation of dielectric constant and dielectric loss with temperature and frequency. Good curve is obtained with increasing temperature for higher frequency like 100kHz or 1kHz. For higher frequency almost no variation of dielectric

constant and dielectric constant with temperature and that is expected as temperature range is low. Low dielectric loss for higher frequencies will be good for application.

For temperature sensing application it is very important to show pyroelectricity. NTO is a ferroelectric material, so it's must have pyroelectric property. To know its temperature sensitivity pyrocurrent measurement is done. Pellets connected with platinum wires using silver paste kept inside the furnace and wires connected to source meter unit (Keithley-2401). Current vs time data is taken with temperature ramping between 600°C to 500°C which shows exponentially increasing or decreasing current w.r.t to temperature ramping. This is called pyrocurrent. This is the evidence of pyroelectricity in NTO material for temperature sensing application.

Nomenclature

NTO	:	Neodymium Titanate
PVA	:	Polyvinyl alcohol
EGTS	:	Exhaust Gas Temperature Sensor
T_c	:	Curie temperature
XRD	:	X-ray diffraction
CIF	:	Crystallographic Information File
COD	:	Crystallographic Open Database
TEM	:	Transmission Electron Microscope
SEM	:	Scanning Electron Microscope
P_r	:	Remnant polarization
P_s	:	Spontaneous polarization
PLD	:	Pulsed Laser Deposition
ICDD	:	International Centre for Diffraction Data

Contents

Chapter 1

1. Introduction

1.1 Electrical properties of functional materials

1.1.1 Ferroelectricity:

Materials that possess switchable spontaneous polarization are called as ferroelectrics. Ferroelectricity was first found in Rochelle salt. Rochelle is the name of the place where the salt was found. The name ferroelectricity is borrowed from ferromagnetism due to the phenomenological analogy. Similar to ferromagnetism (magnetization vs magnetic field) the fingerprint of ferroelectricity is the hysteresis loop (polarization vs electric field). Spontaneously polarized material gives rise an internal depolarization field inside the material. To minimize the internal depolarization
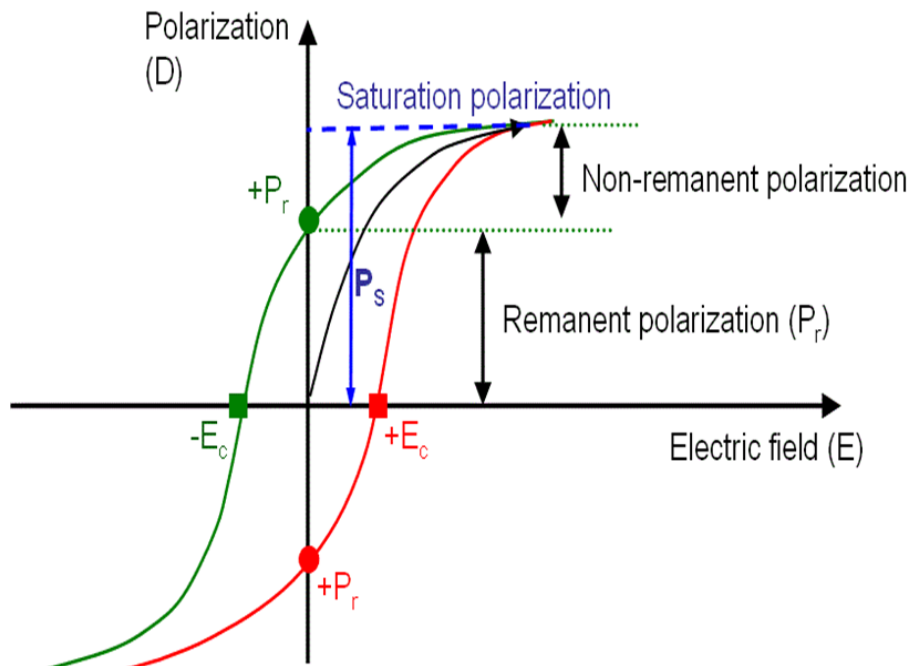
Fig 1.1 Hysteresis loop of ferroelectric material [6]

energy, system breaks into small region of uniform polarization called. This is the origin of domain formation in ferroelectric materials.

Polarization at zero applied field is called remnant polarization (P_r). At coercive field the polarization switches its direction. At the point of spontaneous polarization all the

1

domains are switched in a particular direction and respective opposite side we get a point where opposite polarization is obtained.

One of the essential criteria for exhibiting ferroelectricity is non-centro symmetry or broken spatial inversion symmetry. The simplest structure among the materials that exhibit ferroelectricity is ABO_3 ($BaTiO_3$). Origin of ferroelectricity in barium titanate like structures is due to the rattling of Ti^{4+} cation and the effective structural distortion in TiO_6 octahedral. Strong hybridization between A cation and oxygen anion, weaken the B cation and oxygen interaction. So B cation starts rattling within BO_6 octahedral either upward or downward.
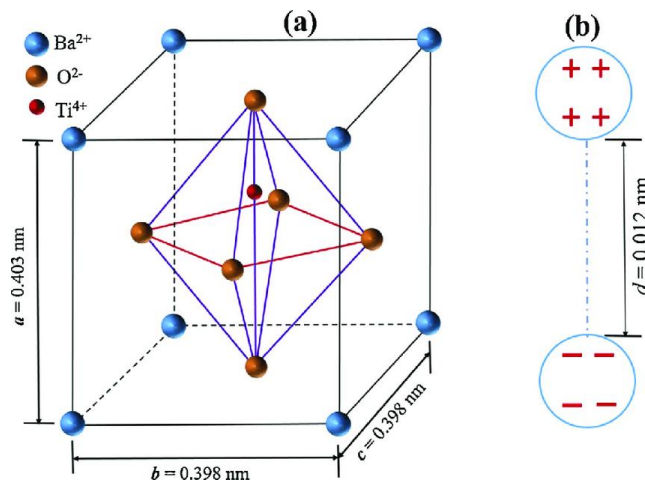
Fig1.2 (a) Rattling of Ti^{4+} ion in TiO_6 octahedral & Fig1.2 (b) dipole moment [7]

Ferroelectric materials possess curie temperature similar to ferromagnetism and they do exhibit a ferroelectric paraelectric transition when heated above T_C. Above the transition temperature(T>Tc) the structure also transforms from non-centro symmetry to centro symmetry. For $BaTiO_3$, curie temperature is 120 °C. $BaTiO_3$ unit cell undergoes various transformation as temperature of the system increases. Room temperature phase is tetragonal and above T_c is cubic.
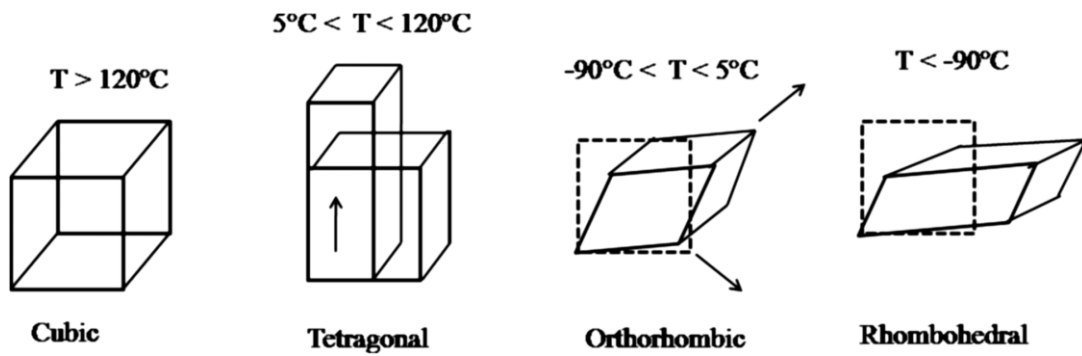
Fig 1.3 ferroelectric and paraelectric phases of BaTiO₃ [8]

Without applying field material is able to maintain polarization direction that can be either upward or downward polarization. There are two stable states with equal energy i.e. two possibility of energy minimization either upward or downward.
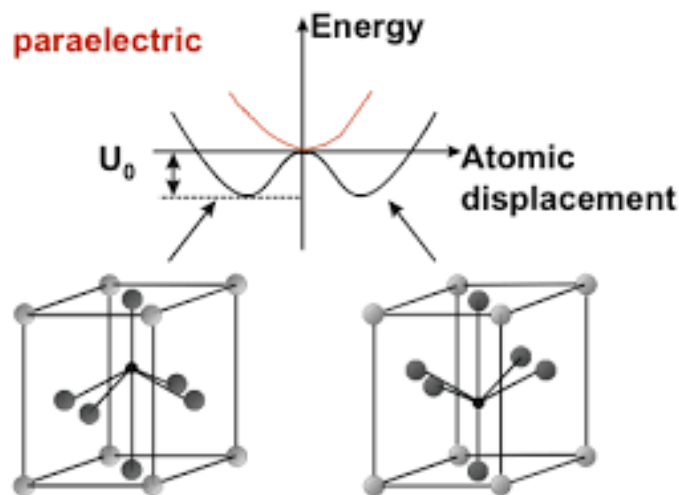
Fig 1.4 Two stable states corresponding to two kind of polarization in BaTiO₃ [9]

Ferroelectric system must undergo structural transformation for going ferroelectric to paraelectric transition as it is a lattice phenomenon. But in ferromagnetic system, there is no any structural transformation involved during ferroelectric to paraelectric transition as it is an electronic phenomenon. This is the key difference between ferroelectricity and ferromagnetism. As it involves lattice, dielectric studies are done for any structural transformation present in sample. Structural phase transformation is studied by looking changes in dielectric constant. Electric susceptibility of ferroelectric system is very large and comes down to very low for paraelectric.

3

Ferroelectric material can be pyroelectric or piezoelectric or dielectric that can be shown in Venn diagram bellow:
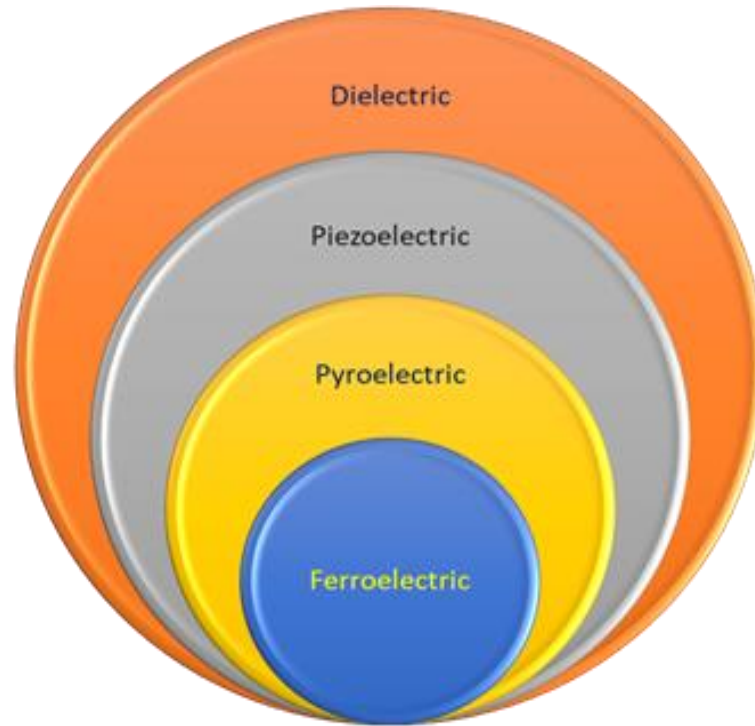
1.1.2 Piezoelectricity:

Greek word "piezo" means pressure i.e. by applying pressure we can generate electricity. This is called direct piezoelectric effect. Reverse is also possible i.e. applying electrical signal we generate deformation / strain in the material which is called converse piezoelectric effect. Curie brothers (Jacques and Pierre Curie) discovered in 1880 this effect in quartz crystal.
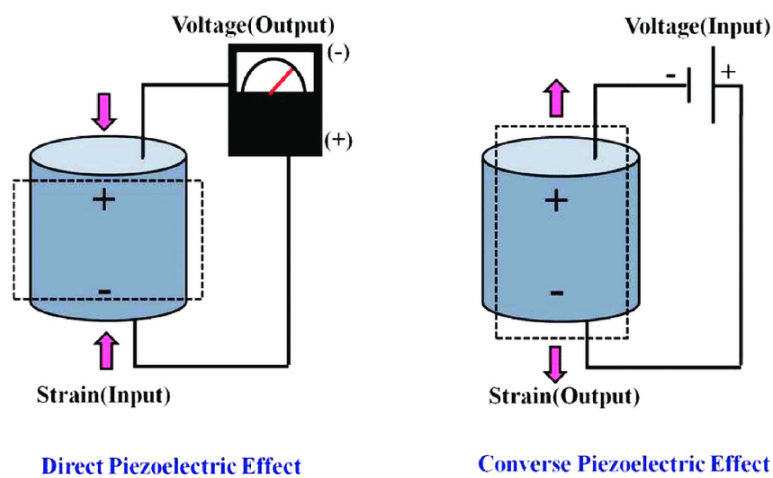
Fig 1.5: Shows schematic of piezoelectric effect [10]

Quartz is not a superior piezoelectric material. Piezo-coefficient is very less. Comparatively BaTiO₃ has high piezoelectric effect. Commonly known very good piezoelectric material is PZT i.e. lead zirconate titanate.
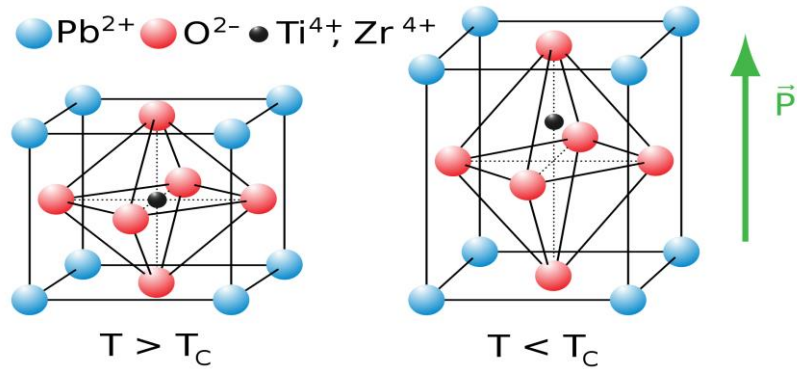
Fig1.6: Shows structure of PZT w.r.t T_c [11]

Among 21 non centro-symmetric point groups 20 are piezoelectric. One is not because its vectorial cancellation of polarization due to its symmetry. i.e. there is no net dipole moment.

Piezoelectric strain constant(d):

Amount of strain developed by applied field

$$d = \partial x/\partial E \qquad (1.1)$$

Piezoelectric voltage constant(g):

Amount of field generated by introducing strain

$$g = \partial E/\partial x \qquad (1.2)$$

Electromechanical coupling factor(k):

This coupling factor tells about efficiency of energy conversion.

k = (stored mechanical energy/input electrical energy)

1.1.3 Pyro electricity:

From the Greek word "pyr" meaning fire, the word pyro came. Pyro electricity was first discovered by Theophrastus (314 BC) in tourmaline. Pyro electricity is basically due to change in temperature there will be change in polarization. By heating or cooling net dipole moment is created. During heating dipoles switches from one direction to another direction that generate displacement current or pyro current. Pyro electric property is determined by measuring the change in spontaneous polarization w.r.t change in temperature.

Pyro electric coefficient:

$$p = \partial P_s / \partial T \qquad\qquad (1.3)$$

where P_s = spontaneous polarization

Primary pyro electric effect:

Change in temperature expands or shrinks the individual dipoles that affects random orientation of dipoles resulting net dipole moment.
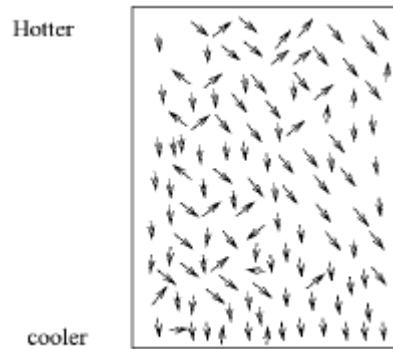
Fig 1.7: Shows primary pyroelectric effect [12]

Secondary pyro electric effect:

Due to change in temperature strain is developed that leads to change in polarization.
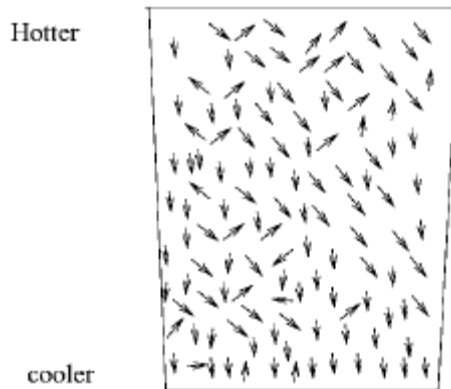
Fig1.8: Shows secondary Pyro effect [12]

1.2 Types of temperature sensors:

Negative temperature coefficient (NTC) thermistor is a resistor that sensitive to temperature. where with increasing temperature resistance decrease. It has high

accuracy (0.05 to 1.5 °C) but the working temperature range is -50 to 250 °C. Due to exponential nature, it's output of an NTC thermistor needs linearization. Other type is resistance temperature detector (RTD). Platinum RTDs show linear output that is highly accurate (0.1 to 1 °C) but working range -200 to 600 °C. RTDs are the costliest temperature sensors. Another type is thermocouple. Accuracy is low, from 0.5 °C to 5 °C but working range is high from -200 °C to 1750 °C.

1.3 Advantages of pyroelectric based sensors:

> Chemically stable as most are metal oxides

> Signal to noise ratio is high

> High responsivity over a broad range of temperature (T_c)

> Devices require no thermal stabilization

> High temperature sensing application (EGTS)

1.4 Importance of high temperature functional material:

Pyroelectric materials are useful for high temperature sensing application. For temperature sensing pyroelectrics can be used in combustion chambers of automobile engines, aeronautical and thermonuclear propulsion system, turbines in cryogenic propulsion units, geothermal sensing in between upper crust and mantle where the temperature range up to 2000°C. In propulsion system it can senses the exhaust gas temperature which decides performance of the engine. Exhaust gas temperature sensor (EGTS) can save the engine from overheating. EGTS senses gas temperature and convert it into voltage signal and send signal to engine control unit (ECU) that protect the engine components from harmful radiations.

1.5 Objectives:

Major objectives of my project are:

> Preparation of ferroelectric material with (T_c>900°C) for high temperature sensing application.

> Synthesis and structural analysis of high temperature ferroelectric ($Nd_2Ti_2O_7$ - NTO).

> Temperature dependent study of dielectric and pyroelectric properties of NTO bulk ceramics.

Chapter 2

2. Literature Review:

2.1 Study on NTO material:

Pyroelectric based high temperature sensing technology is important in automotive, aerospace, chemical and material processing [1]. So far, no piezoelectric material performing as sensor above 800°C [1]. Ferroelectric materials are interested in high temperature sensing technology because of pyroelectric properties.

Primary requirement for using ferroelectric material as high temperature sensing application is high curie temperature (T_c). Neodymium Titanate ($Nd_2Ti_2O_7$) also called NTO has high curie temperature (1480°C) [1]. Pyroelectric based high temperature application determined by the thermal depoling characteristics. Thermal depoling depends on ferroelectric domain structure, phase transitions and internal mechanical stress [1]. Cause of high T_c in NTO material [1]:

➢ The material has only 180° ferroelectric domains.

➢ Ferroelectric to paraelectric transition of NTO involves the displacement of the whole sublattice of the TiO_6 octahedron.

So, NTO material is attractive in high temperature pyroelectric devices.

Neodymium Titanate has monoclinic structure with space group $P2_1$. Paraelectric phase ($>T_c$) is orthorhombic with space group Cmcm [1].
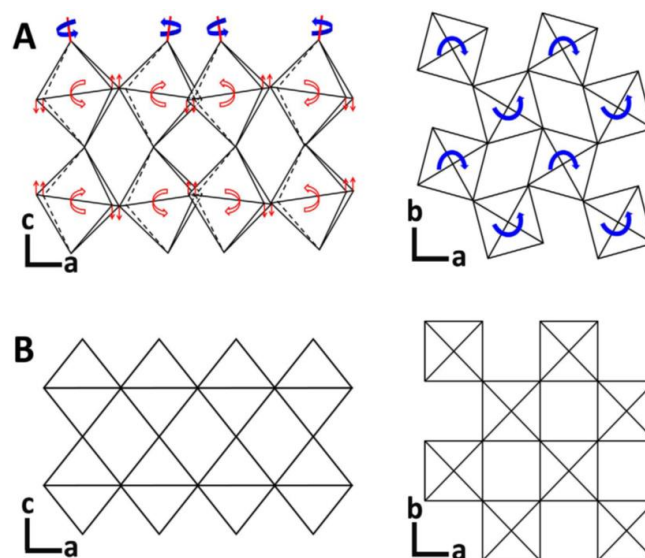

Fig 2.1: TiO_6 octahedron rotation and tilting projected along b- and c-axis in (A) ferroelectric phase and (B) paraelectric phase [1]

8

The ferroelectric spontaneous polarization arises due to the rotation of TiO_6 octahedron around c-axis and tilting around b-axis (Fig 2.1). Spontaneous polarization shows only in b-axis, that generates only 180° domains. Ionic displacement occurs along b-axis, which is the origin of ferroelectricity in NTO material. Generally, there is shape change due to switching of non 180° domains that creates a large internal mechanical stress in poled materials [1]. This internal stress with thermal disturbance is the cause of thermal depoling. This effect is not there with material only 180° switching [1].

2.2 Solid state synthesis of NTO material:

$Nd_2Ti_2O_7$ material is prepared by mixed oxide route which is called solid state synthesis process. In this process high purity (>99.9%) powders of Nd_2O_3 and TiO_2 were wet mixed (in molar ratio 1:2) for 8 hours with zirconia balls. After that powder calcined at 1100 °C for 4 hours. Again wet mixed for 12 hours. Then 15 mm diameter pellet prepared by mechanical pressing of powder. Pellets sintered in the range 1375°C to 1400°C for 4 hours. Starting mixed powders was pale blue and after calcination color changed to pale violet. Sintered pellet were dark violet with theoretical density about 93-95%. Single phase neodymium titanate of calcined powder was confirmed by x-ray diffraction analysis. It is reported [2] that good quality single phase NTO is prepared by solid state process.

2.3 Structural study of NTO material:

Layered type perovskite structure of NTO contains TiO_6 octahedral and Nd, Ti and O ions (Fig.2.2). Layers are stacked along 'b' axis with interconnecting Nd-O bonds. Due to the TiO_6 octahedron rotation and tilting respectively along c and b-axis, Nd and Ti ions displaces from centre of symmetry which is the cause of net polarization in the crystal [3].

Scheunemann and Müller-Buschbaum (1975) (abbreviated as SMB) determined structure of NTO based on XRD data. It was reported that NTO has monoclinic structure and P2$_1$ space group. Lattice parameters are a=7.6 Å, b=5.4Å, c=26 Å, β=98.4˚ [5].
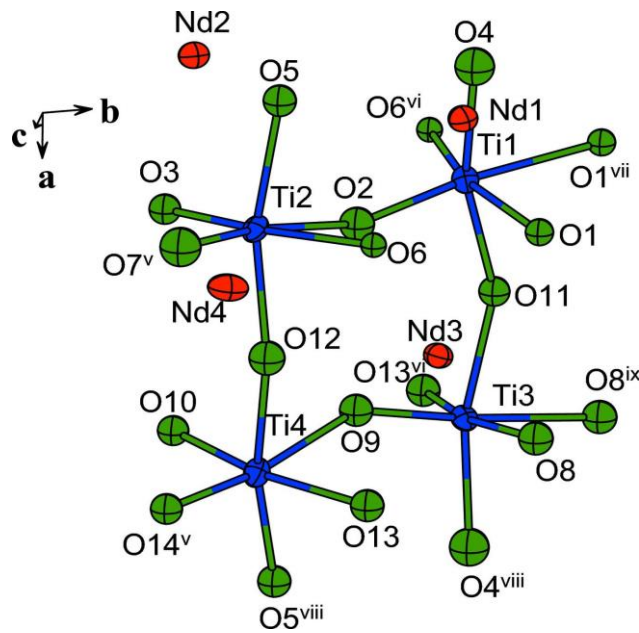
Fig2.2 Structure of NTO containingTiO$_6$ octahedron [3]
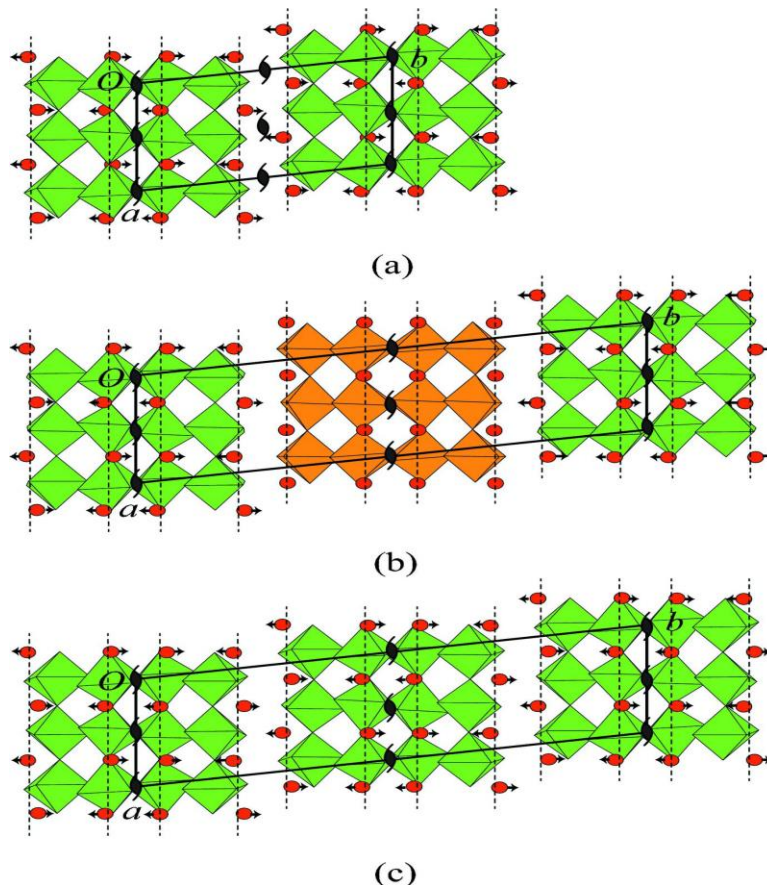
Fig 2.3. Comparison of NTO structures, (a) recent study, (b) Scheunemann & Müller-Buschbaum (1975), (c) Harvey et al. (2005). Two types of perovskite layers are shown using green and orange coloured TiO$_6$ octahedra, respectively. The small black arrows are the displacements of Nd atoms shown by red spheres along b* with respect to the dotted lines which are parallel to a [3].

SMB [3] structure had two types of perovskite-like slabs with octahedral green and orange colored. The green-colored slab is similar to the study, that can be understood by octahedral tilting about b* and the displacement of Nd atom along b* as shown by arrows. The orange-colored slab in the SMB structure has very small octahedral tilting about b* in addition with very little Nd atom displacements along b*. The different types of slabs stacking alternately along b states about the doubled unit cell in the SMB structure.

Harvey et al. [3] (2005) (abbreviated as HWLSR) studied a $Nd_2(Zr_{1-x}Ti_x)_2O_7$ solid solution and reported a monoclinic structure for the last member $Nd_2Ti_2O_7$ based on refinement by the Rietveld method. The unit cell dimensions and symmetry of the HWLSR structure has similar to that of SMB. SMB and HWLSR structures are not similar as HWLSR contains the same green-type slabs.

The conclusion is that the HWLSR [3] structure model is very similar to the present one. Also, it is difficult to neglect the possibility of two monoclinic unit cells for $Nd_2Ti_2O_7$ at room temperature like the SMB structure.

2.4 Properties study on NTO material:

$Nd_2Ti_2O_7$ is a family member of perovskite-type layered ferroelectric materials. Other members are $La_2Ti_2O_7$, $Ca_2Nb_2O_7$ and $Sr_2Nb_2O_7$. Kimura et all showed that single crystals of NTO had piezoelectric and electro-optic properties and had a Tc around 1500°C. Marzullo and Bunting studied that NTO had a relative permittivity of 37, a high dielectric Q value [2].

Fig 2.4 TEM micrograph showing twinned domain pattern in a single grain of NTO, sintered at 1450°C (doped with 3 mole % Nb_2O_5) [2].

TEM studies exposed the presence of twinned domain structures confirms the ferroelectric nature of NTO [2].
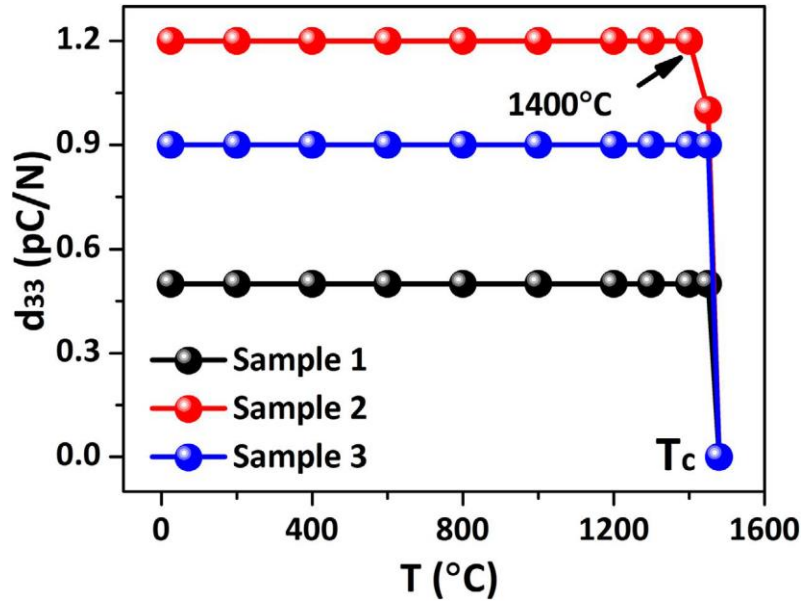
Fig 2.5 showing variation of d$_{33}$ with annealing temperature [1]

Fig.2.5 shows the piezoelectric constant d$_{33}$ behavior of Nd$_2$Ti$_2$O$_7$ ceramics with the annealing temperature. The value of d$_{33}$ showed very stable up to 1400 °C and became zero at about 1480 °C, which is the Curie temperature of Nd$_2$Ti$_2$O$_7$. Due to the different poling conditions of these three samples the d$_{33}$ is varied. Due to different electrical breakdown there were different poling field. Electrical field is increased from 10 kV/mm up to electric breakdown [1]. So, the poling field of each sample is decided by the breakdown field, which can affect the piezoelectric property.

Total spontaneous polarization (P$_s$) of NTO was calculated based on the ionic displacements using Shimakawa's model- [1]

$$P_s = \sum_i \frac{m_i \Delta x_i Q_{ie}}{V} \tag{2.1}$$

Where m$_i$ is the site multiplicity and Δx$_i$ is the atomic displacement along the c-axis, Q$_{ie}$ is the ionic charge of the ion, and V is the volume of the unit cell.

12
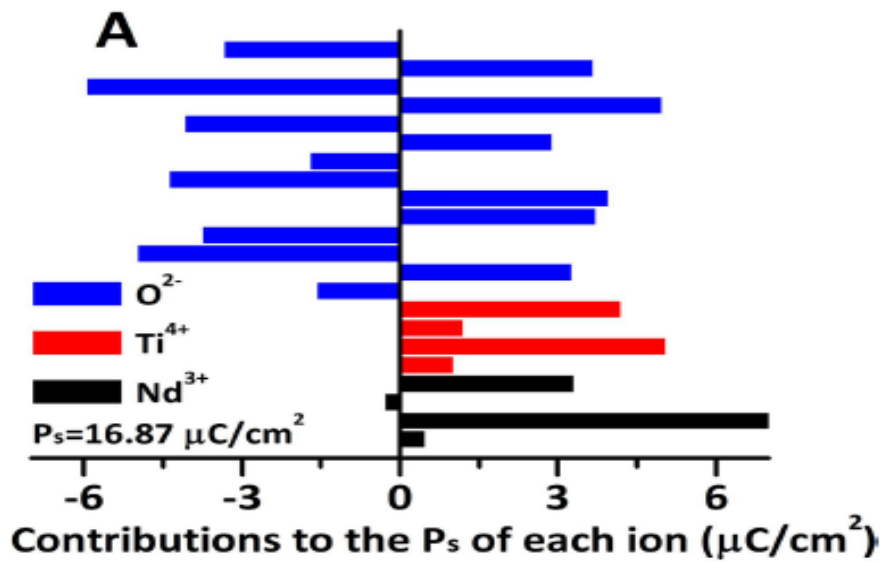
Fig.2.6 Showing Ionic contribution to total spontaneous polarization (P_s) of each ion of NTO

[1]

The dielectric studies reveal that the ferroelectric to paraelectric phase transitions (T_c) occurs at around 1481°C (T_c). The dielectric studies with a mistmatch between heating and cooling tells about the thermal hysteresis of ferroelectric to paraelectric transition of $Nd_2Ti_2O_7$, similar to a first order transition. However, NTO serves as a super stable ferroelectric with a large T_C indicating it as a potential candidate for the high temperature applications.

Chapter 3

Experimental details:

3.1 Solid state synthesis method:

Solid state reaction route is widely used to prepare crystalline ceramic oxides. Factors affecting the rate of reaction in this technique are surface area, reactivity, solid state diffusion and thermodynamic free energy change of reaction. Primary materials are chosen depending on reaction condition and nature of product. After weighing stoichiometrically, the primary materials are mixed and using agate mortar and pestle mixture is grinded for 4-5 hours with volatile organic liquid (acetone or 2-propanol). During grinding liquid evaporates after 15 minutes. In this way fine powders are achieved which enhances the reaction rate surface area increases. Later the fine powders were transferred in to a high purity alumina crucible which is chemically inert to reactants and the reaction was carried out in a high temperature muffle furnace in normal atmosphere.

Flowchart of this method is given bellow:

Weighing of metal oxides with stoichiometric amount $\longrightarrow$ Mixing with acetone or 2-propanol using mortar and pestle (5-6 hours) $\longrightarrow$ drying $\longrightarrow$ Calcination $\longrightarrow$ Grinding and Mixing with PVA binder $\longrightarrow$ Pelletization $\longrightarrow$ sintering.

3.2 Synthesis of NTO material by solid state route:

Nd_2O_3 and TiO_2, in the molar ratio 1:2 are mixed

⬇

Wet Grinding with 2-Propanol of the mixture for 4 h

⬇

Calcination at 1250°c for 4 h

Dry grinding for 30 minutes

Ball milling with 200 rpm for 11 h

Mix with PVA binder

Palletization (pressing)

Pellets are sintered at 1400˚C for 5 hours where heating and cooling rates are usually 5˚C/min
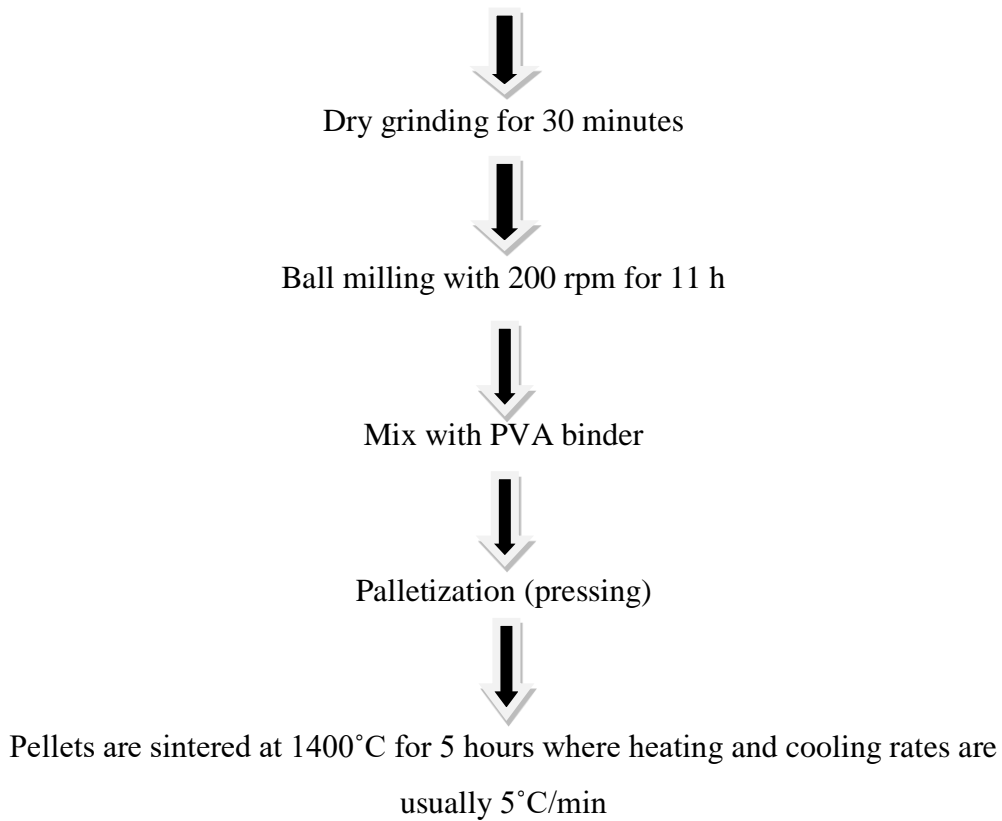
Fig 3.1: Flowchart of preparation of NTO sample by solid state synthesis method

Primary materials:

Neodymium oxide(Nd_2O_3) and Titanium oxide(TiO_2) powders [high purity 99.99%, manufactured from Sigma Aldrich] are the primary materials for preparation of Neodymium Titanate ($Nd_2Ti_2O_7$).

Weighing and mixing:

It is very important to measure the weights of primary materials for maintaining stoichiometric ratio. For preparation of 8 gm of NTO powder

   a) Nd_2O_3 :   5.424 gm

   b) TiO_2 :   2.575 gm

$$Nd_2O_3 \ + \ 2\,TiO_2 \ = \ Nd_2Ti_2O_7$$

Wet grinding with 2-propanol of mixture (5.424 gm Nd_2O_3 & 2.575 gm TiO_2) is done for four hours. Hand grinding with mortar & pestle is done up to which fine powders are not achieved.

Calcination:

Calcination is a heat treatment process to remove the oxides of carbon and for the reaction to take place among the reactant oxides. It removes volatile fraction and gives desired phase of the material. Dried mixed powder was calcined at 1250°C for 4 hours. After calcination powder was grinded for 30 minutes and information about phase is obtained by XRD.
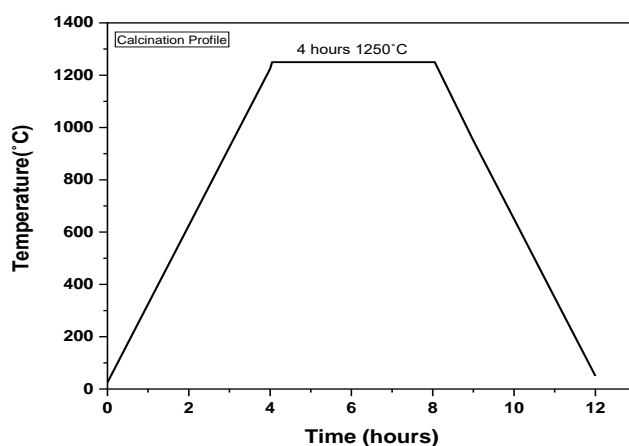
Fig.3.2. Calcination profile of NTO at 1250° C

3.3 X-ray diffraction (XRD technique):

XRD is a powerful technique to characterize crystalline materials. It can give information about crystal structure, phase, unit cell dimension, sample purity etc.

Max Von Laue discovered that the inter-planar spacing (1-5 Å) in a crystal lattice is similar to the 3D diffraction grating for X-ray wavelengths (1-10 Å). Using X-ray Von Laue, W.H Bragg and his son W.L. Bragg independently demonstrate how to find crystal structure, lattice parameters of the crystal from X-ray diffraction experiment. They took different treatment for x-ray diffraction but fortunately results of these two treatment are same. Bragg treatment based on model and Laue's treatment based on scattering from each lattice point in the crystal.

Bragg basically assume that:

➢ Crystal has set of equispaced parallel planes which is called d-spacing.

16

- ➢ When x-ray falls on the crystal, it reflected from each plane following reflection rule.

- ➢ Reflected rays will interfere resultant will be constructive interference. Depending on the path difference there may be destructive interference. Path difference = 2dSinθ = nλ, that must be followed. Bragg select those diffracted rays which follow reflection rule and will interfere constructively.
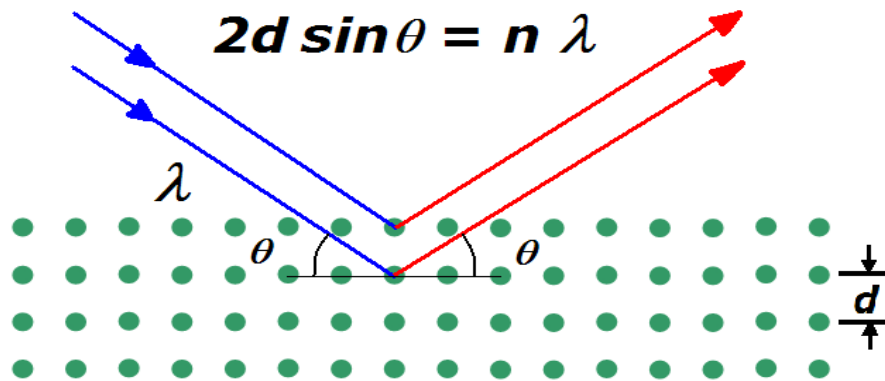
Fig3.3: Bragg's law for x-ray diffraction [13]

X-ray diffractometer circle or goniometer contains three major part an X-ray source, a sample stage, and an X-ray detector. When filament is heated, electrons are produced which accelerated towards target material by applying voltage. When accelerated electrons hit the target material, it can knock and take out inner shell electrons of the target material. So, to fill the inner shell vacancy higher shell electron jump to lower shell as a result energy difference comes out as electromagnetic wave whose wavelength in the range of X-ray. The spectra consist of different components like K_α and K_β. Again K_α consists of K_{α_1} and K_{α_2}. K_{α_1} has a slightly shorter wavelength and twice the intensity as K_{α_2}. The specific wavelengths are characteristic of the target material (Cu, Mo, Co).
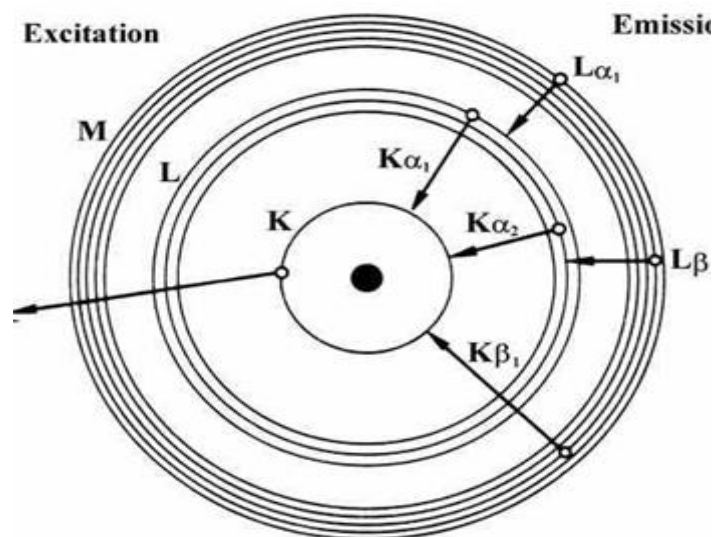
Fig3.4: shows K_{α_1}, K_{α_2} emissions [14]

Copper is one of the common target material for XRD, with CuK_α radiation = 1.5418Å. These X-rays which are coming out are completely divergent beam. X-rays are collimated by slits and directed onto the sample. Detectors also have slits and filters to pass only particular X-ray beam K_α. When the X-rays incident on the sample and follows the Bragg's condition, constructive interference takes place and a peak in intensity occurs. A detector detects this X-ray signal and shows output on computer monitor. The geometry of an X-ray diffractometer is such that the sample rotates at an angle θ while the X-ray detector rotates at an angle of 2θ. For typical powder diffraction, data is taken at 2θ from 20° to 90° angles.

XRD of calcined powder was done to check the desired phase is formed or not. Scanning range of 2θ was from 20 ° to 90° and the source of X-ray radiation was Co ($\lambda_1 = 1.7891$ Å, $\lambda_2 = 1.7932$Å).

3.4 Ball milling:

Ball milling is one type of grinder or mechanical mixing process. It works on the principle of collision and abrasion. There is a hollow cylindrical jar with partially filled hard balls (ZrO_2 or steel), inside which powder is poured. When the system rotates due to the centrifugal force balls drop from the top of the shell and also there will be collision between the balls and between the balls material squeeze. So particles become finer and finer. Ball milling is done to resize the particle. There are two types

of ball milling wet and dry milling. In wet milling powder put in solvent where as in dry milling no liquid is used, only powder is put in standard ball milling.
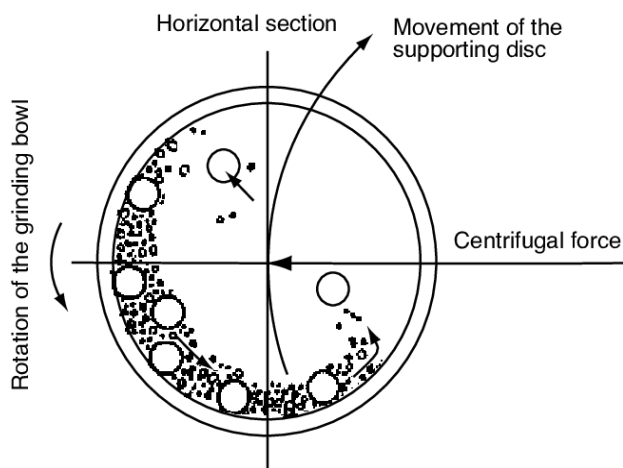
Fig3.5. schematic of ball Milling [15]

Fig 3.6. shows NTO sample within ball milling cylindrical vessel. Wet Ball milling (mixed 2-propanol) of sample was done with 200 rpm for 11 hours to make fine powder.

3.5 Pelletization:

Palletization is a process of compaction of fine powder material into shape of pellet. Before compaction powder is mixed with PVA binder and grind it for 30 minutes using mortar and pestle. After grinding 4 gm powder is weighted in mass balance to make a pellet which can be used as target for PLD. Two pellets are prepared one of 16.96 mm diameter and width 2.98 mm, another pellet of 8.83 mm diameter and 1.62

mm width. Big pellet is made for PLD target and small pellet for property study. Pressure is applied about 3-4 ton/mm^2 for 1 minute.

Fig3.7: Spectek instrument for making pellet [16]

3.6 Sintering of pellet:

Sintering is a unique process to manufacture ceramic products. Main purpose is to densify the material. It provides shape of the ceramic materials. In this process powder is heated to high temperature bellow its melting point which provide activation energy to the system to release excess energy due to high surface area, so that cohesive force binds the particles together and a strong bond is developed. Driving force for sintering basically decreasing the excess surface energy associated with the free surfaces of the fine powder. This can be done by in different ways:

> Reduction of total surface area by increasing average size of the particles i.e. coarsening of particle size Replacement of high energy solid-vapor interface by low energy solid-solid interface i.e. creation of grain boundaries.

Image3.8. of pellet sintered at 1400°Cfor 5 hours using high temperature furnace with heating and cooling rates are 5°C/min.

3.7 SEM imaging of pellet:

Scanning electron microscope (SEM) is a powerful technique to know surface morphology of sample by using electrons. Working principle based on scattering of electron. Main components of SEM instrument are source of electron, electromagnetic lenses, sample stage, electron detector and computer (shown in fig.3.9(b)). Electrons produced in electron gun are accelerated and focused towards the sample by electromagnetic lenses. When electron hit the sample, produces different signals which are auger electron, secondary electron, backscattered electron, characteristic X-ray, transmitted electron. Different signals as result of interaction of electrons with sample at different depth (Shown in fig.3.9(a)). Secondary electrons coming from very near (5nm depth from surface) to the sample surface creates high resolution image of sample surface. Backscattered electrons coming from more depth (400 nm from surface) creates image of less resolution than secondary electron imaging. Characteristic X-ray comes when electron knocked out an inner shell electron from sample, so that high energy electron fills that vacancy and results release of energy as electromagnetic radiation. Due to high depth of field SEM produces three-dimensional image to understand the surface morphology of the sample.
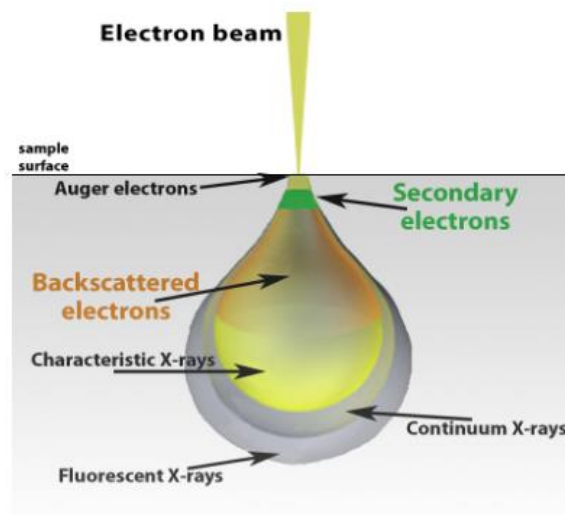

Fig.3.9(a) Electron –matter interaction [18]

SEM image of NTO pellet (on the surface) was taken to know how the particles are densely packed. Images are taken with different magnifications, regions and working distances. Two types of imaging are captured

- ➢ Secondary electron imaging

- ➢ In –lens detector imaging
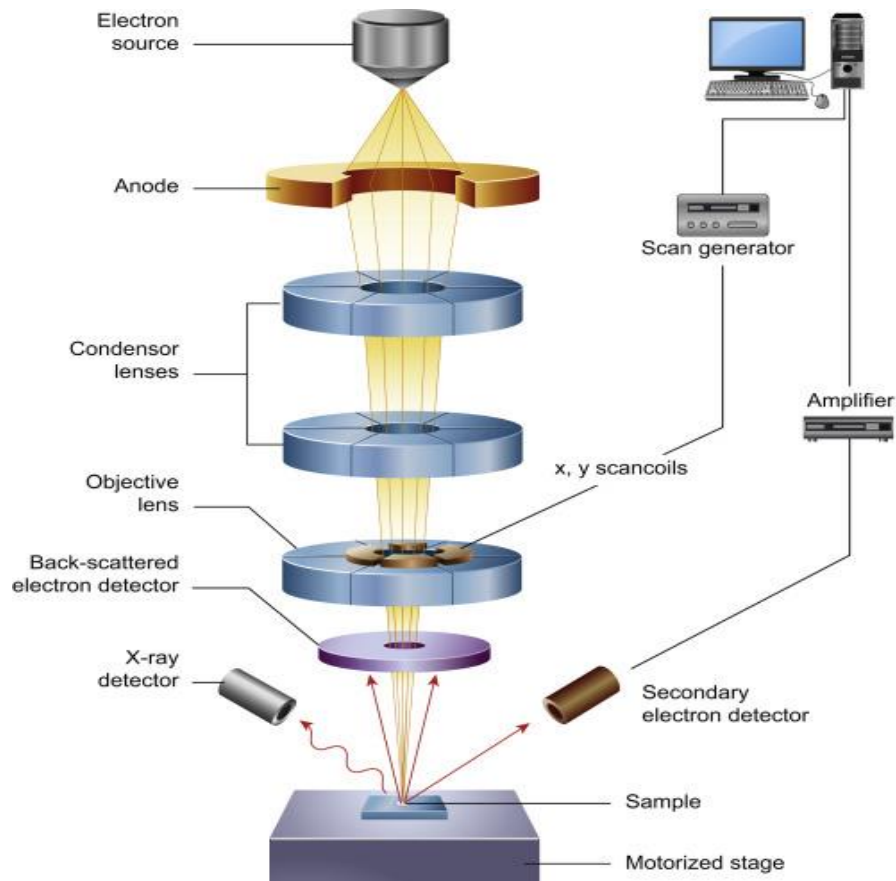
Fig.3.9(b) Components of SEM [17]

3.8 E-beam deposition:

Electron beam deposition is one type of physical vapor deposition technique for thin film. There are crucibles of different materials (copper, platinum) act as source material. When power is applied e-beam is generated from tungsten filament by thermionic emission. The e-beam accelerated and directed towards the source material with high kinetic energy. Path of the e-beam towards the source material is controlled by the electromagnets. When e-beam strikes the source material, kinetic energy converted to heat energy. High vacuum is created within the deposition chamber to reduce the collision between the particles. The material starts melting and after applying sufficient power material evaporate and deposit on the substrate.\

Fig.3.10 schematic of e-beam deposition [19]

Platinum (Pt) of 40 nm thickness was deposited on both sides of pellet as electrode material for dielectric study. A vacuum of 4.5 x 10^{-5} mbar was created inside the deposition chamber by a set of rotary pump and turbo pump. Pressure reading by penning gauge and p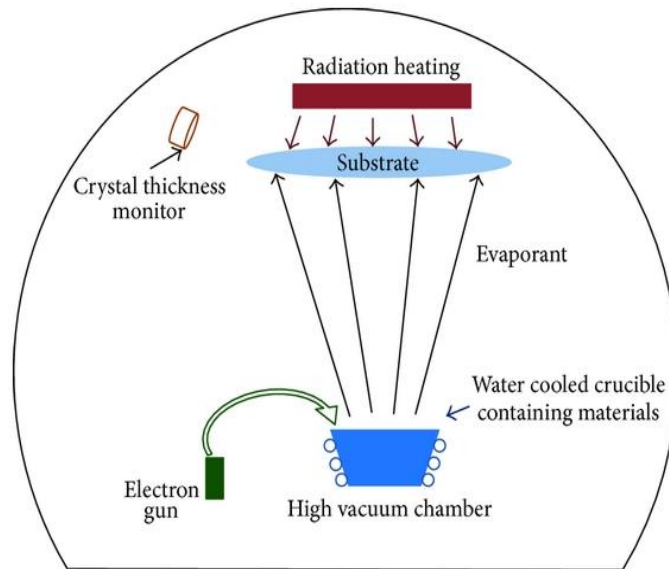irani gauge: PR1-4.9 x 10^{-3} mbar, PR2-2.2 x 10^{-2} mbar, PNG-6.0 x 10^{-6} mbar. Initial rate was 0.5 Å/s and final thickness was 0.45 KÅ for 40 nm deposition. During experiment power increased from 0% to 18% to start deposition. After reaching 18% of power material evaporated and deposition rate increased to 1.4-1.8 Å/s.

3.9 High temperature dielectric study:

Dielectric materials basically insulator that can be polarized applying electric field. It has high resistivity like insulator. When field is applied center of positive and negative charge separated i.e. dipole moment is produced. Dipole moment per unit volume is called polarization. Dielectric material is characterized by dielectric constant or relative permittivity. Higher dielectric constant leads to higher polarization. Due to polarization dielectric materials can store electrical energy. Common use of dielectric is as capacitor. For parallel plate capacitor capacitance is given bellow:
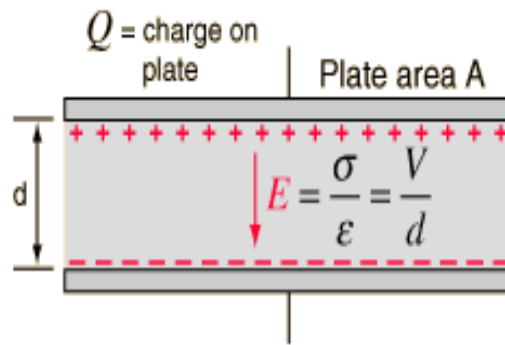
Fig3.11: schematic of parallel plate capacitor [20]

$$C = k\varepsilon_0 A/d \qquad (3.1)$$

Where,

C = Capacitance

d = plate separation

A = plate area

K = relative permittivity of the dielectric medium

ε_0 = permittivity of free space = 8.854 x 10^{-12} F/m

Polarizability is a property of dielectric materials which is defined as the ability of a material to polarize by applying electric field. Polarization is directly proportional to the electric field:

$$P \alpha E \rightarrow \quad P = \alpha E \qquad (3.2)$$

Where proportionality constant α = polarizability

Contributions to polarizability comes from four different factors:

1.   Electronic polarizability (α_e): Light elementary particle electron can polarize even at high frequency (10^{15} Hz) i.e. electron can follow variation of electric field at frequency of 10^{15} Hz. So polarization at high frequency is due to polarization of localized electrons. Without applied field electrons clouds are distributed around nucleus in such a way that centre of positive charge and the centre of negative charge situated at the same point. But when dielectric is subjected to an external electric field, Lorentz force (-eE) displaces the nucleus and the electron cloud from their equilibrium position. Positively charged nucleus moves in the direction of field and negatively

24

charged electron cloud moves opposite to the direction of the field. Also coulomb attractive force acts on the system when they try to separate. When these two forces become equal and opposite then nucleus and electron cloud will be in equilibrium with separated by a distance i.e. dipole moment is created in atom.

$$\alpha_e = 4\pi\varepsilon R^3 \tag{3.3}$$

Electronic polarization is proportional to the volume of the atoms in the material and it is independent of temperature

2.   **Ionic polarizability (α_i):** Separation of cations and anions with applied electric field occur in the frequency range $10^{12} - 10^{13}$ Hz. When ions are displacing w.r.t applied electric field, restoring force proportional to the displacement of ions acts on the system that try to pull backward to their mean equilibrium positions.

$$\alpha_i = \frac{e^2 E}{w_0^2} \left(\frac{1}{m} + \frac{1}{M}\right) \tag{3.4}$$

Ionic polarization is independent of temperature, inversely proportional to the reduced mass and square of the angular frequency.

3.   **Dipolar polarizability (α_d):** It occurs in polar dielectrics. Reorientation of dipoles or molecules take place in the frequency range $10^6 - 10^{11}$ Hz. Here polarization is much slower than the electronic and ionic polarization.

$$\alpha_d = \frac{\mu^2}{3KT} \tag{3.5}$$

Dipolar polarization is inversely proportional to the absolute temperature of the material.

4.   **Space charge polarizability (α_s):** Space charge is basically local uncompensated charge. At very low frequency ($<10^3$ Hz) long range charge migration can take place which contributes to polarizability.

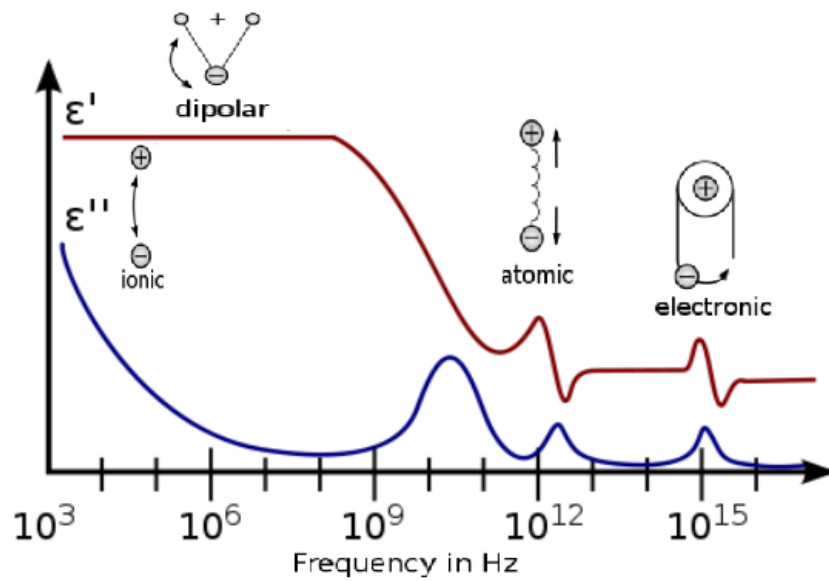$$\alpha = \alpha_e + \alpha_i + \alpha_d + \alpha_s \tag{3.6}$$

Fig.3.12. frequency dependence dielectric constant (ε^{I}) and dielectric loss (ε^{II}) [21]

At high frequency contribution to polarization coming from only electronic polarizability and at low frequency all the different mechanism of polarization will contribute to overall polarization and hence dielectric constant increases. Polarizability varies with frequency due to different time scale of response of different mechanism of polarization.

Electronic and ionic polarizability are independent of temperature. When temperature increases orientation polarizability decreases as it affects the tendency of dipoles to align along direction of field but space charge polarizability increases as it helps in diffusion of ions.

Dielectric loss is important as it indicates how much energy is absorbed or lost from the system. Low dielectric loss materials are good for application.

Chapter 4

Results and discussions:

4.1 XRD data analysis:

XRD of calcined powder was done to check the phase purity. The diffraction pattern confirmed NTO single phase. Peak positions were matched with ICDD data of NTO material.
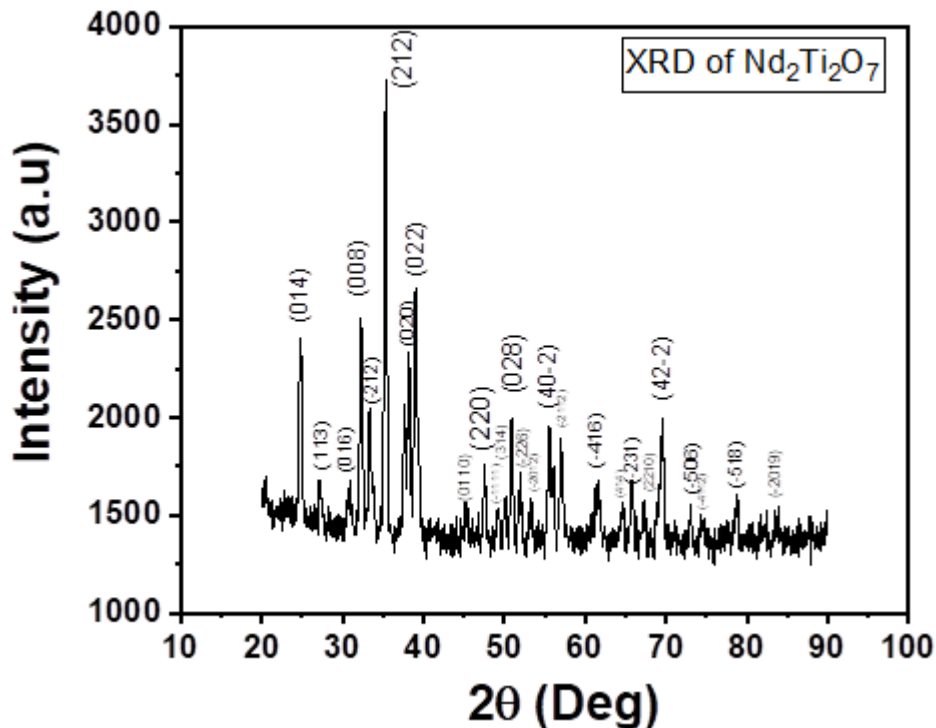
Fig.4.1 shows XRD pattern of NTO powder after calcination at 1250°C

It is reported that [1]:

➢ It has monoclinic crystal structure with $Nd_2Ti_2O_7$ phase

➢ Space group-$P2_1$

➢ Lattice parameter: a=7.6 Å, b=5.4Å, c=26 Å & β=98.4˚

Average particle size is calculated from Scherrer's formula which is about 25 nm.

$$D = K\lambda / \beta Cos\theta \hspace{3cm} (4.1)$$

Where,

D is the crystallite size of nanoparticle

K is a constant (0.94)

λ is the wavelength of X-ray (Cok$_\alpha$ = 1.7891 Å)

β is the FWHM

θ is the half diffraction angle of the centre of the peak in degree.

The d-spacing for major diffracted set of planes are tabulated in bellow from Bragg's law:

$$2dSin\theta = n\lambda \qquad (4.2)$$

Where,

d = spacing between the parallel planes or inter planar spacing

θ = half of the diffraction angle

n = order of the diffraction pattern

λ = wavelength of X-ray

2θ	θ	SINθ	COSθ	FWHM (DEG.)	β (RAD)	βCOSθ	PARTICLE SIZE (NM)	D-SPACING (Å)
24.80	12.40	0.2113	0.976	0.3812	0.0066	0.00644	25	4.2
32.28	16.14	0.2779	0.960	0.3749	0.0065	0.00624	25.8	3.2
35.32	17.66	0.3033	0.952	0.3877	0.0067	0.00637	25.2	2.9
39.04	19.52	0.3341	0.942	0.4125	0.0071	0.00668	24.1	2.6
50.92	25.46	0.4298	0.902	0.4045	0.0070	0.00631	25.5	2.0
69.60	34.80	0.5707	0.821	0.5315	0.0092	0.00755	21.3	1.5

4.2 Unit cell image:

The structure of $Nd_2Ti_2O_7$ contains perovskite-type slabs consisting of TiO_6 octahedron and Nd, Ti, O ions. The slabs are stacked along c with interconnecting Nd—O and Ti-O bonds.

Space group - $P2_1$

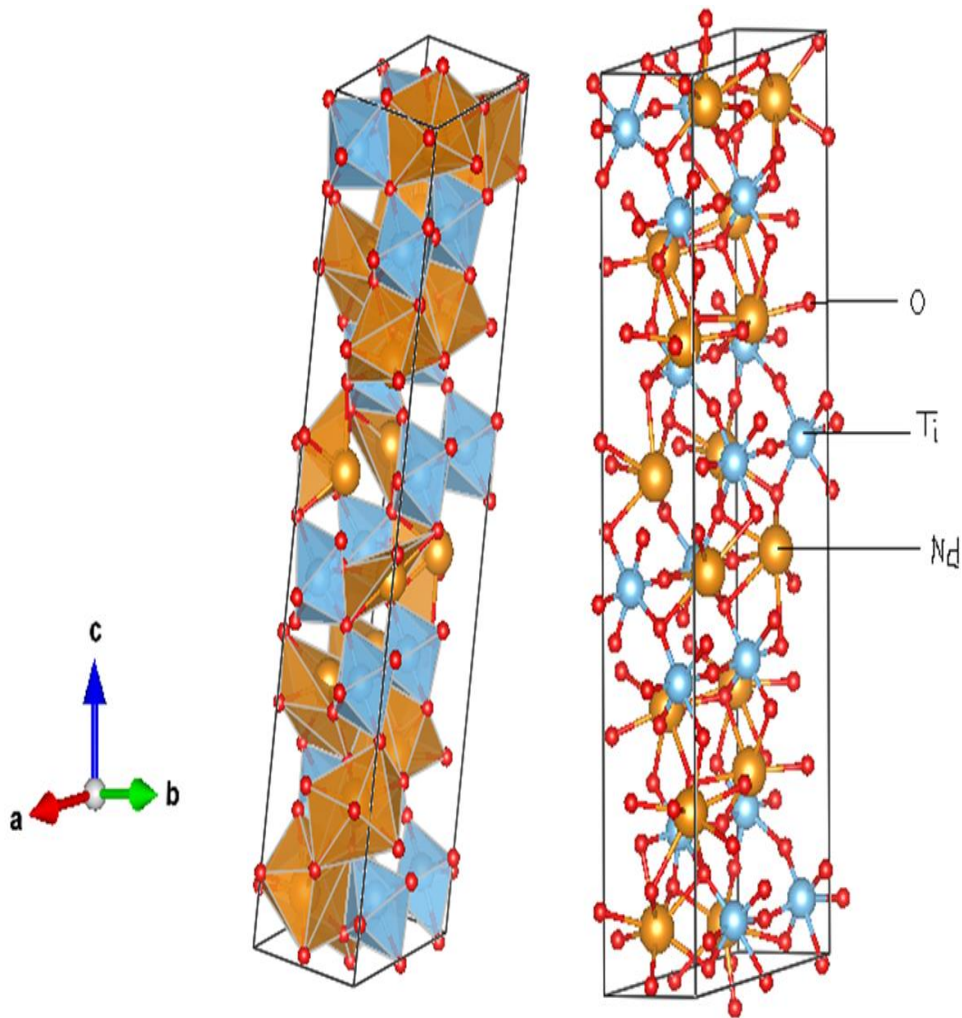Lattice parameter: a = 7.6 Å , b = 5.4Å , c = 26 Å,   β = 98.4

Fig.4.2 Unit cell image of NTO material showing atomic arrangements and TiO_6 octahedron created by Vesta software.

4.3. Fullprof refinement:

Principles of Rietveld refinement:

Rietveld refinement is a structural refinement technique that uses least square method to refine a theoritical pattern until matches with observed pattern. Least square is a statistical method that create a line of best fit by minimizing the sum of squares of mathematical function. A square is calculated by squaring the distance between data point and the regression line. The weighted sum of squares [23] is given by

$$\sum W_i(y_i^{obs} - y_i^{cal})^2 \qquad (4.3)$$

Where $W_i = \frac{1}{y_i^{obs}}$ statistical weight which is used in fitting of the observation

y_i^{obs} = observed intensity at the ith step

y_i^{cal} = calculated intensity at the ith step

Basically informations like crystal structure, space group, lattice parameters are given to the software and based on this software generates a pattern which is called model or calculated pattern. Experimental data pattern is called observed pattern. If the observed and calculated patterns are not matched then the input informations are changed to reduce the difference between them. Difference between calculated and observed pattern must be as minimum as possible. Once certain number of instruction are given then it generate pattern similar to that of experimental pattern.then whatever informations are given to the software is sample's information. The minimization is done using the reliability index parameters such as weighted profile factor, Bragg R-factor, chi^2, goodness of fitting. All the parameters are used as numerical criteria to check the quality of fitting between calculated to the observed diffraction data. Chi^2 value is the squared ratio between the weighted profile R-factor from refinement and expected value of the R-factor. Bragg R-factor is is agreement of reflection intensities between calculated model and observed X-ray diffraction data. Goodness of fitting defines the quality of agreement between observed and clculated pattern.

Reitveld refinement parameters:

In Fullprof there are different parameters by refining of which best fitting can be achieved. These parameters decides height, width and position of the peaks. The parameters are refined one by one accordingly. Scale factor, temperature factor, Lorentz factor matches height of the intensity profile. Shape parameter matches the shape of the peaks. Lattice parameters and atomic co-ordinates decide the peak positions. Occupancy parameter tells about probability of finding an atom at a specific atomic site. It is defined as the ratio of the number of equivalent atoms in a set of equivalent positions and maximum site multiplicity of the space group.
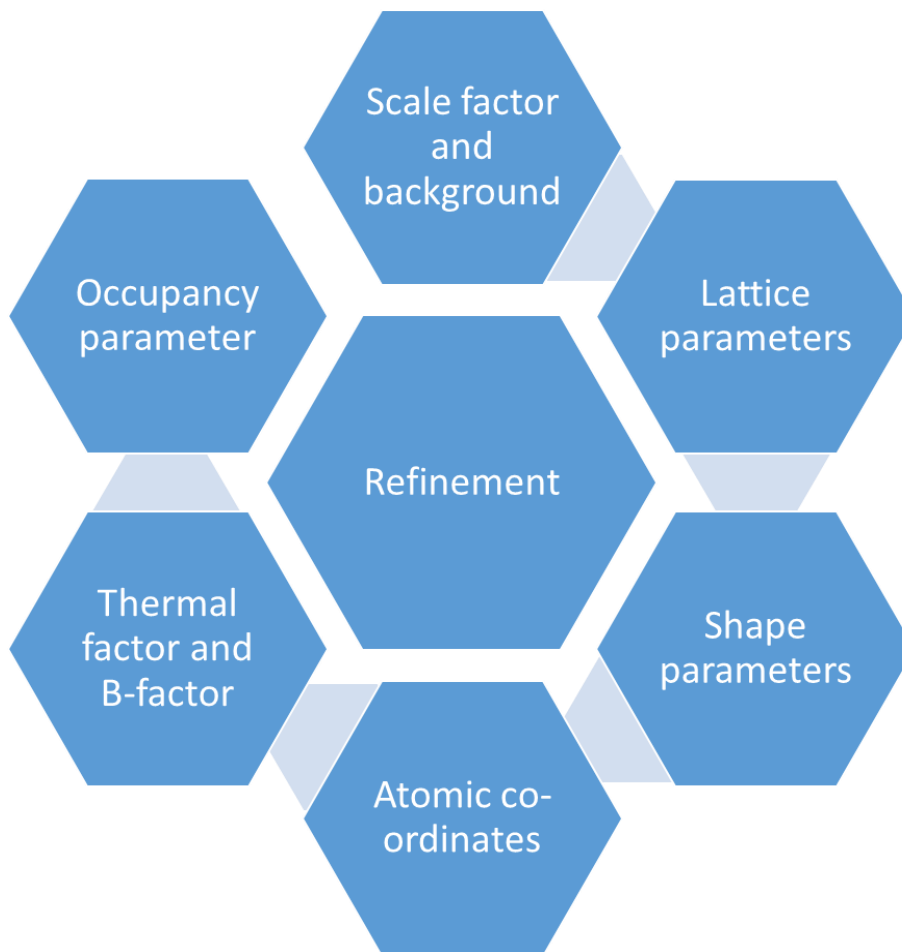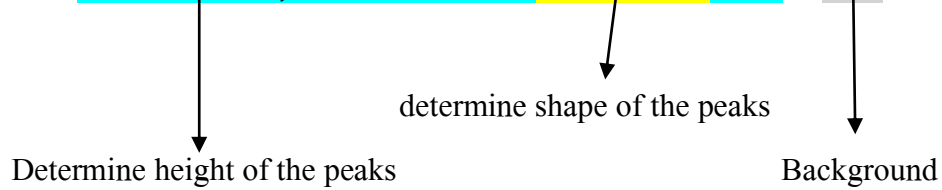
Diagram shows Rietveld refinement parameters

Calculated intensity:

$$I_i^{cal} = S_F \sum_{j=1}^{N\ phases} \frac{f_j}{V_j^2} \sum_{k=1}^{N\ Peaks} L_k |F_{k,j}|^2 S_j(2\theta_i - 2\theta_{k,j}) P_{k,j} A_j + bkg_i \qquad (4.4)$$

determine shape of the peaks

Determine height of the peaks   Background

Where i= number of steps

j= number of phases

k= kth reflection

31

Factors affecting intensity:

$$I_i^{cal} = S_F\sum(f_j/V_j^2)\sum L_k|F_{k,j}|^2 S_j(2\Theta_i - 2\Theta_{k,j})P_{k,j}A_j + bkg_i$$

Lorentz factor

Background

Absorption

Scale factor

Profile shape

S_F = Beam intensity

f_j = volume fraction

V_j = cell volume

Preferred orientation

Structure factor

Background:

$$I_i^{cal} = S_F\sum(f_j/V_j^2)\sum L_k|F_{k,j}|^2 S_j(2\Theta_i - 2\Theta_{k,j})P_{k,j}A_j + bkg_i$$

In XRD background originated from diffraction of non-characteristic emissions of X-ray tube, amorphous container, air scattering etc. So the XRD pattern arises from both the sample and background contributions. In Fullprof there are different way to model the background. It can be modelled by linear interpolation method or polynomial function of 2Θ. When x-rays are incident on sample, lattice vibration occurrs and that vibration scatters in a diffuse manner. This reduces intensity of the peaks and also appears in the background. It is necessary to model the extra non-crystalline contributions for refinement of crystalline structure. This is done by using higher order polynomial function of 2Θ.[22]

Scale factor:

$$I_i^{cal} = S_F\sum(f_j/V_j^2)\sum L_k|F_{k,j}|^2 S_j(2\Theta_i - 2\Theta_{k,j})P_{k,j}A_j + bkg_i$$

Scale factor is a constant factor that scales the intensities of calculated to the observed pattern. Basically matches the height of the intensity profiles of calculated to the observed values.

Lorentz factor:

$$I_i^{cal} = S_F \sum (f_j/V_j^2) \sum L_k |F_{k,j}|^2 S_j(2\theta_i - 2\theta_{k,j}) P_{k,j} A_j + bkg_i$$

When a set of planes are diffracting then it is assumed that planes are perfectly oriented w.r.t Bragg angle. But in reality there are two categories of Bragg angle. One is diffracting plane which oriented exactly to the Bragg angle and other is slightly different from Bragg angle. Both have their own contributions in the XRD pattern. Based on this angular distribution i.e. angle of rotation of crystal until diffraction occurs, fraction of crystallites which contributes the angular distributions and other geometrical factors Lorentz factor is calculated.[26]

Structure factor:

$$I_i^{cal} = S_F \sum (f_j/V_j^2) \sum L_k |F_{k,j}|^2 S_j(2\theta_i - 2\theta_{k,j}) P_{k,j} A_j + bkg_i$$

It is the atomic scattering factor from all the atoms in the unit cell. It is defined as the ratio of amplitude of wave scattered by an atom to the

amplitude of wave scattered by an electron. It basically tells how atomic co-ordinates contributes to the intensity. Expression of structure factor [25]

$$|F_{k,j}|^2 = m_k |\sum_{n=1}^{N} f_n e^{-\frac{B_n \sin^2 \theta}{\lambda^2}} (e^{2\pi i(hx_n + ky_n + lz_n)})|^2 \qquad (4.5)$$

Absorption factor:

$$I_i^{cal} = S_F \sum (f_j/V_j^2) \sum L_k |F_{k,j}|^2 S_j(2\theta_i - 2\theta_{k,j}) P_{k,j} A_j + bkg_i$$

Absorption is a property of material. Basically when electromagnetic radiation interacts with matter then one of the phenomenon is absorption [23]. To account this there is absorption factor which modifies intensity.

Debye-Waller temperature factor:

As the atoms are vibrating about their mean equilibrium position, scattering by atom is reduced. The magnitude of displacement of vibration is defined by Debye-Waller temperature factor [24]:

$$B = 8\pi^2 U^2 \qquad (4.6)$$

Where

U^2 is the mean square displacement of vibration.
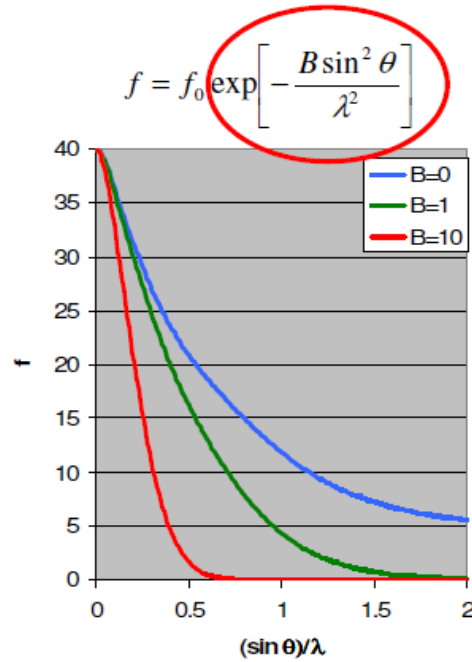

Fig4.3: shows B accelerate the decreases [24]

Isotropic vibration means the displacement of atoms are equal in all three direction and anisotropic vibration means displacement of atoms are not equal in all direction. This temperature factor decreases the probability of scattering by atoms.

Preferred orientation:

$$I_i^{cal} = S_F \sum (f_j/V_j^2) \sum L_k |F_{k,j}|^2 S_j(2\theta_i - 2\theta_{k,j}) P_{k,j} A_j + bkg_i$$

It arises whenever there is a tendency of orientation of the crystallites in a particular direction. The condition is crystallites must be non-spherical. It produces systematic distortion in the reflection intensities [22]. This can be modelled by preferred orientation function. March-Dollase function [25] shows the best performance for the crystal structure study.

$$P_{k,j} = \frac{1}{m_k} \sum_{n=1}^{m_k} (P_{MD}^2 \cos^2 \alpha_n + \frac{\sin^2 \alpha_n}{P_{MD}})^{-\frac{3}{2}} \qquad (4.7)$$

Where, P_{MD} is the March-Dollase parameter

Summation is for all equivalent hkl reflections (m_k)

α_n is the angle between the preferred orientation vector and the crystallographic plane hkl.

It modifies the intensity profile. At first the intensities are taken by assuming ideal powder sample that contains randomly oriented crystallites. But crystallites may not be randomly oriented, so its effect is modelled by suitable function.

Profile shape:

$$I_i^{cal} = S_F \sum (f_j/V_j^2) \sum L_k |F_{k,j}|^2 S_j(2\theta_i - 2\theta_{k,j}) P_{k,j} A_j + bkg_i$$

Common profile shape functions are Gausian, Lorentzian, Pseudo-Voigt. Lorentzian has longer tail than Gaussian. Lorentzian represents better for smaller crystallites. Most of the XRD profiles are Pseudo-Voigt i.e. mix of Gaussian and Lorentzian. Basic peak shape parameter is FWHM. Peak shape depends on sample's mosaicity, crystallite size, micro-strain and instrumental error. Caglioti formula represents variation of FWHM with angle 2θ

$$w^2 = W + V\tan\theta + U\tan^2\theta \tag{4.8}$$

Where, U, V, W are the peak width parameters related to the crystallite size and strain broadening. Rietveld shows that this refineable parameters (U, V, W) describe perfectly FWHM with angle [23].

Quality of refinement:

Quality of the refinement is decided by the R-indices and goodness of fitting [25]. weighted profile factor R_{wp} is important. Its absolute value does not depend on the absolute value of the intensities but depend on background. For high background it is easy to get very low value. If the number of peak increases, then it is difficult to reach low values.

$$R_{wp} = \sqrt{\frac{\sum_{i=0}^{n}[w_i(I_i^{exp} - I_i^{calc})]^2}{\sum_{i=0}^{n}[w_i I_i^{exp}]^2}}, \qquad w_i = \frac{1}{\sqrt{I_i^{exp}}} \tag{4.9}$$

$$R_{exp} = \sqrt{\frac{(N - P)}{\sum_{i=0}^{n}[w_i I_i^{exp}]^2}} \tag{4.10}$$

Where R_{exp} is the minimum possible value of R_{wp} that can be achieved by using certain number of refine able parameters.

Goodness of fitting, **GOF = Rwp/Rexp** [25], that cannot be less than 1.
For good refinement GOF < 2.

Refinement strategy:

Effects in diffraction pattern	Origin in crystal structure model
Wrong peak positions	Unit cell dimensions Zero-shift
Wrong intensities	Scale factors, atomic co-ordinates, thermal factors, preferred orientation
Wrong peak width	FWHM, crystallite size, micro-strain

Possible cautions:

- ➢ First get a good experimental result
- ➢ Know information of about sample as much as possible
- ➢ Refine parameters one by one
- ➢ First try to fit the spectrum as much as possible
- ➢ Don't stop at first result
- ➢ Zoom in the plot and try to understand how to get good fitting
- ➢ Check fitting criteria and try to minimize the difference as much as possible

Results of refinement:

The figure 4.4 is at first when the program was run Bragg R-factor, R_F-factor and Chi^2 exhibiting relatively larger values.

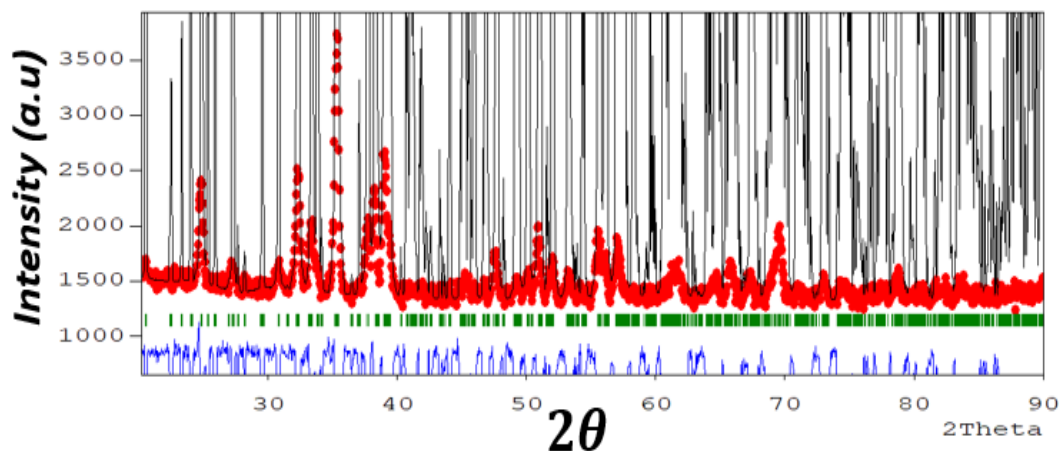Bragg R-factor=3936, R$_F$-factor=566.8

Figure 4.4. refinement performed with non-optimized fitting parameters showing poor quality of fit.

Where, Black line – calculated pattern

Red line – observed pattern (experimental)

Blue line – the difference between calculated and observed pattern

Green line – peak positions

When scale factor and background is refined then the difference reduced significantly.

Intensity profiles matches but shapes of calculated peaks do not match with observed pattern. chi^2 = 13.7. Bragg R-factor=58.18 R$_F$-factor=43.27
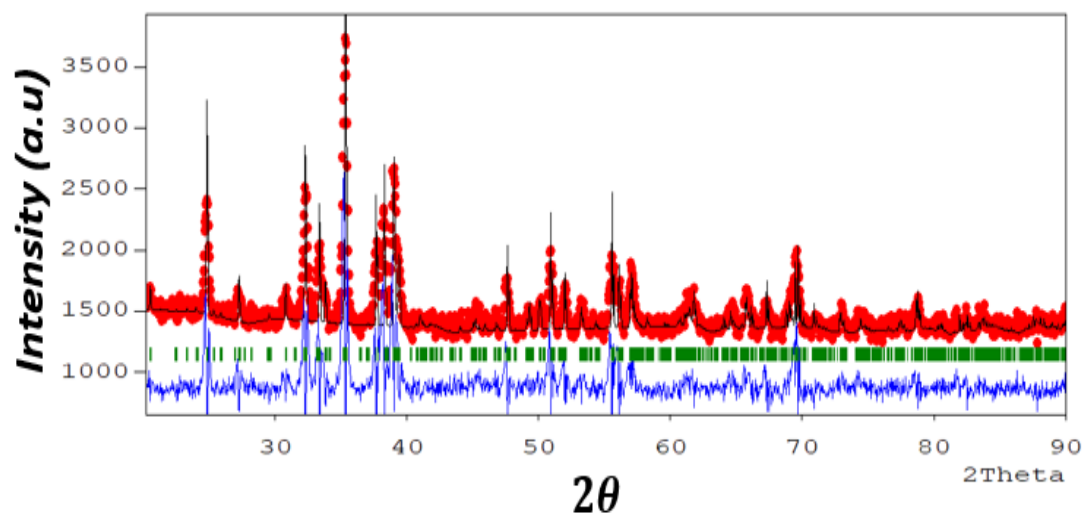

Figure 4.5. refinement performed with scale factor and background.

After that shape parameters in FWHM (U, V, W) are refined then peak shapes of calculated pattern matches with the experimental pattern.

Bragg R-factor=8.96   Chi^2 = 1.43
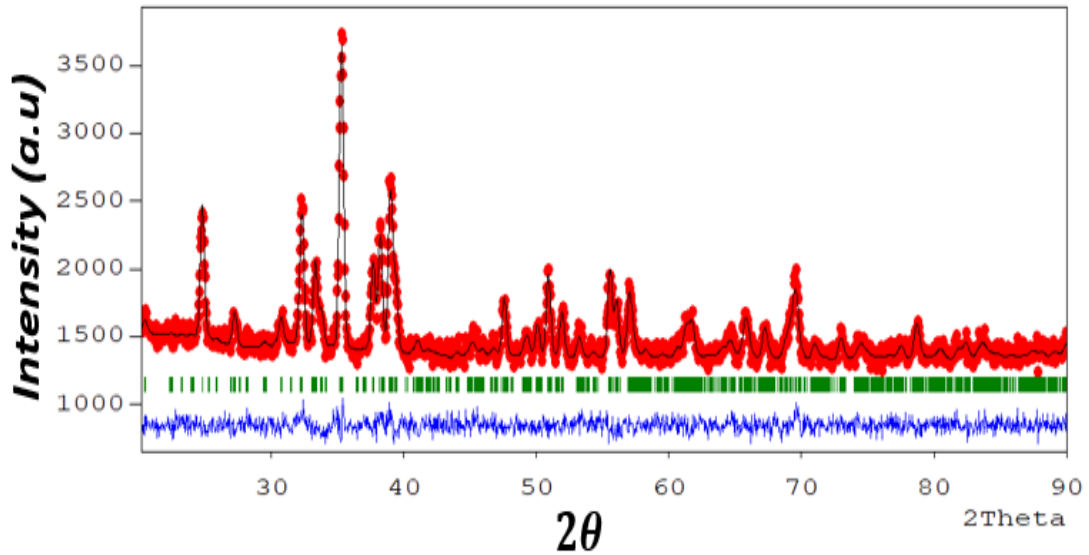
R$_F$-factor=7.78

Figure 4.6. refinement performed with FWHM parameters.

Preferred orientation and instrumental is refined to get good fitting.

Bragg R-factor=8.64   chi^2 =1.37
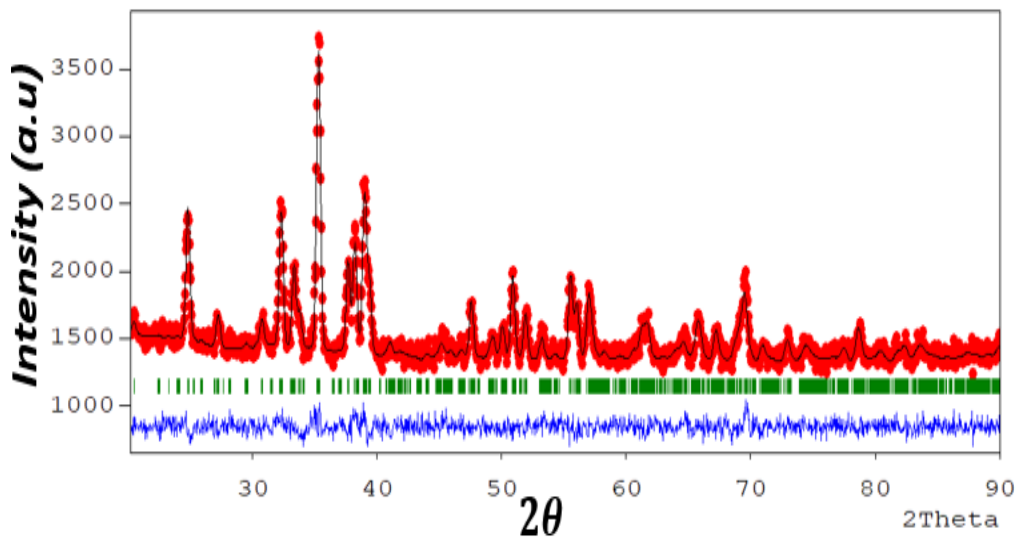
R$_F$-factor=7.84

Figure 4.7. refinement performed with preferred orientation parameters.

Finally, atomic co-ordinates, occupancy parameter, B-factor are refined to get better output.

Bragg R-factor=6.03 $Chi^2 = 1.34$

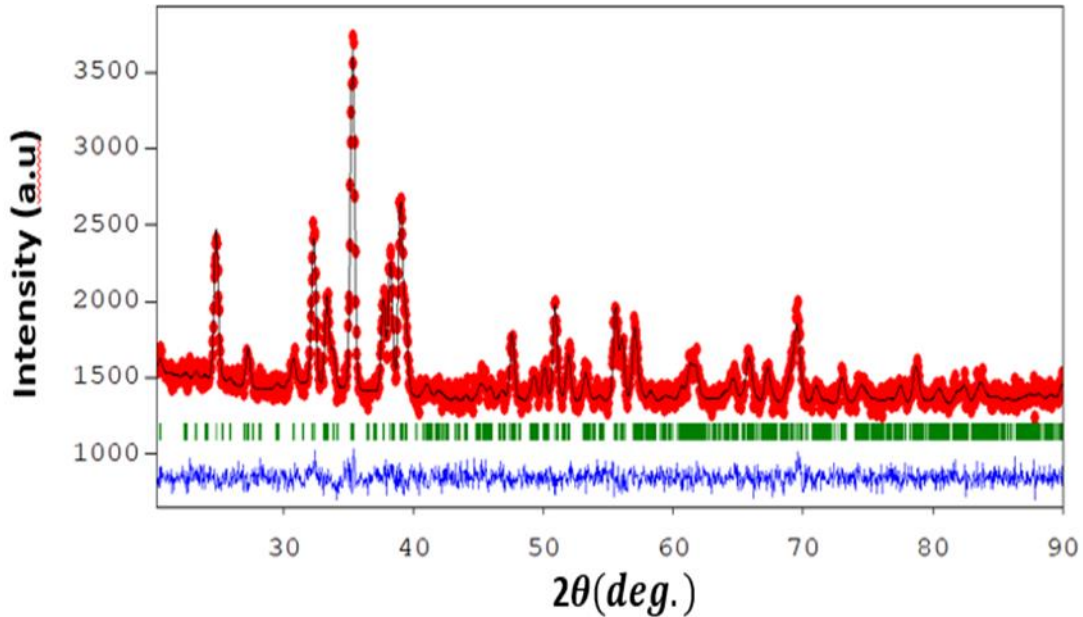R_F-factor=5.62   GoF = 1.16

Figure 4.8. refinement performed with atomic coordinates, temperature factor and occupancy parameters showing good fitting.

4.5 SEM image analysis:

After sintering SEM images on surface of pellet was captured to know the densification of pellet. It shows how particles are bonded to each other. Two types of imaging i.e. secondary electron imaging(SE) and in-lens detector imaging are done with different magnification, region and different working distances.
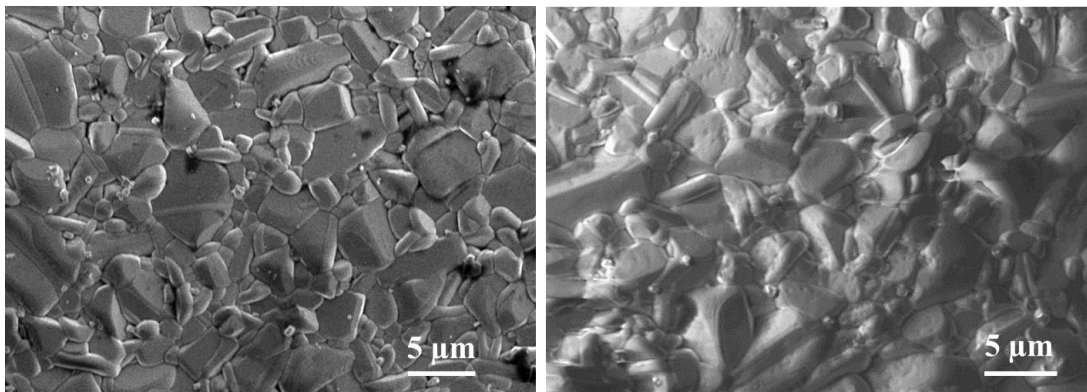

Fig4.9: (a) SE imaging, (b) In-lens detector imaging

Experimental density of pellet is determined.

Density of pellet

$d = \frac{m}{v} = 3.663/0.63 = 5.81 \text{ gm/cm}^3$

4.6 EDS analysis:

EDS of pellet is done for a particular selected area. Shows there was no loss of any element during sintering and stoichiometry is maintained.
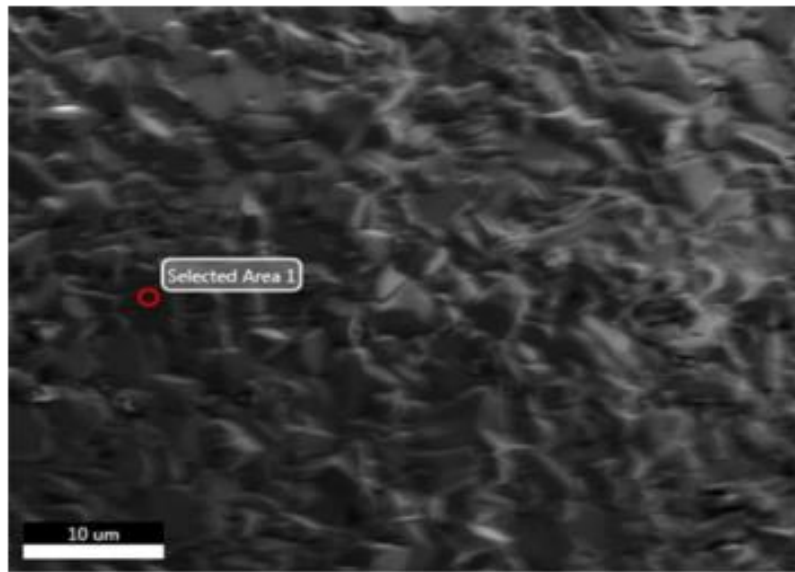

Fig4.10: shows selected area at 20 kV and x2000 magnification for analysis

Element	Weight %	Atomic %
Nd	4.7	0.6
Ti	2.4	0.8
O	92.9	98.6

4.7 High temperature dielectric studies:

Dielectric studies were performed in two steps one from room temperature to 300°C and later from room temperature to 750°C.

i) In first experiment silver paste is used on both sides of the pellet as electrode material and copper wire is connected on both sides for connecting to the adapters. Applied voltage was 0.8 volt. Data was taken from 300°C -60°C within the frequency range 50 Hz – 1 MHz.
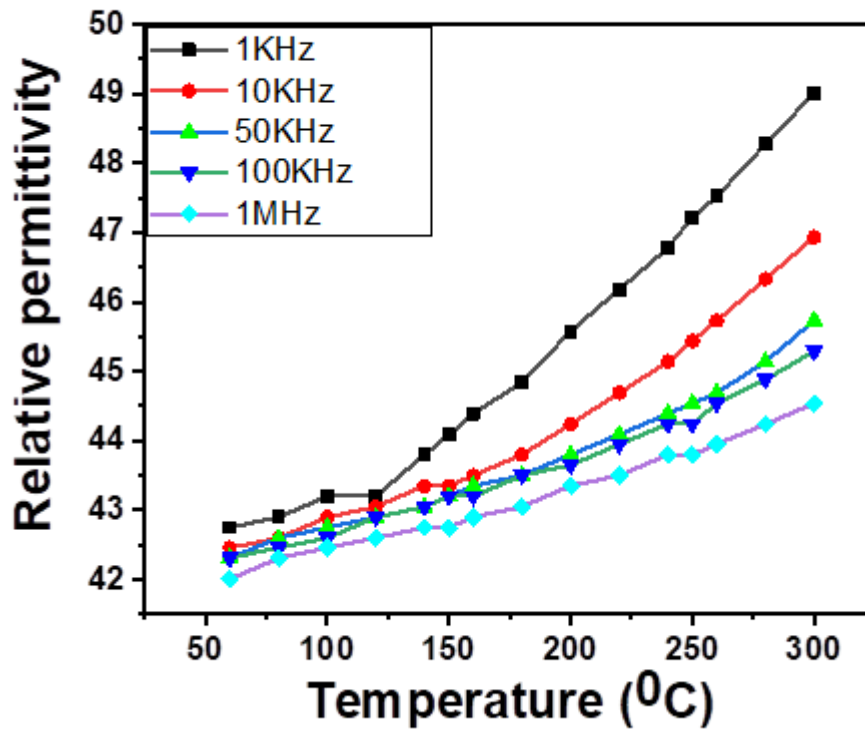
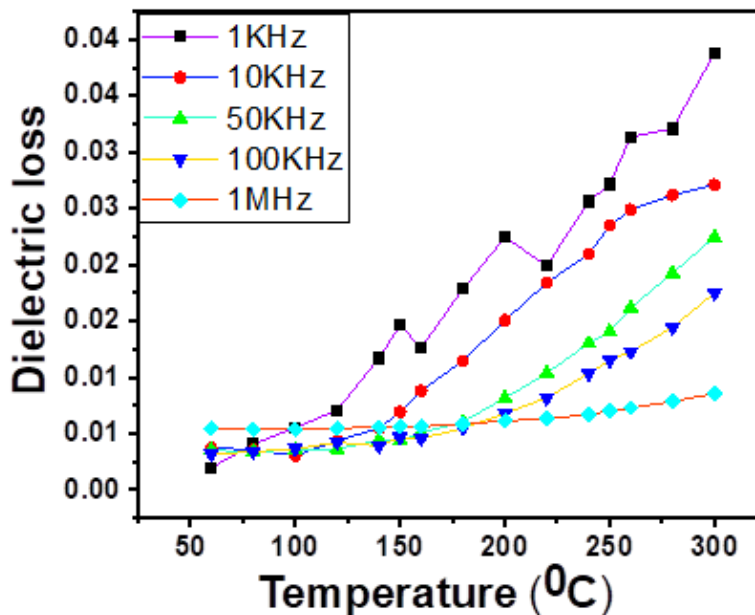Fig4.11: shows variation of relative permittivity or dielectric constant with temperature and frequency.

Fig4.12: shows variation of dielectric loss with temperature and frequency

ii) In this experiment platinum is deposited as electrode material on both sides of pellet by e-beam deposition technique. Platinum wires are connected on both sides of pellet

to connect to the adapter. Applied voltage is 0.5 volt. Data is taken from 750°C – 50 °C within the frequency range 100 Hz – 1 MHz.
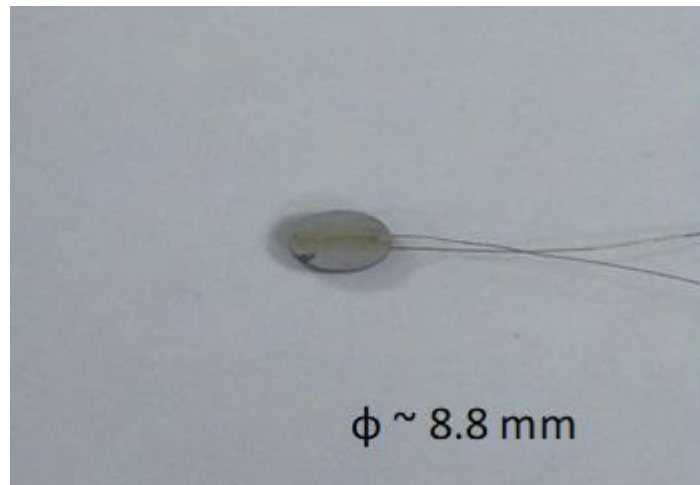

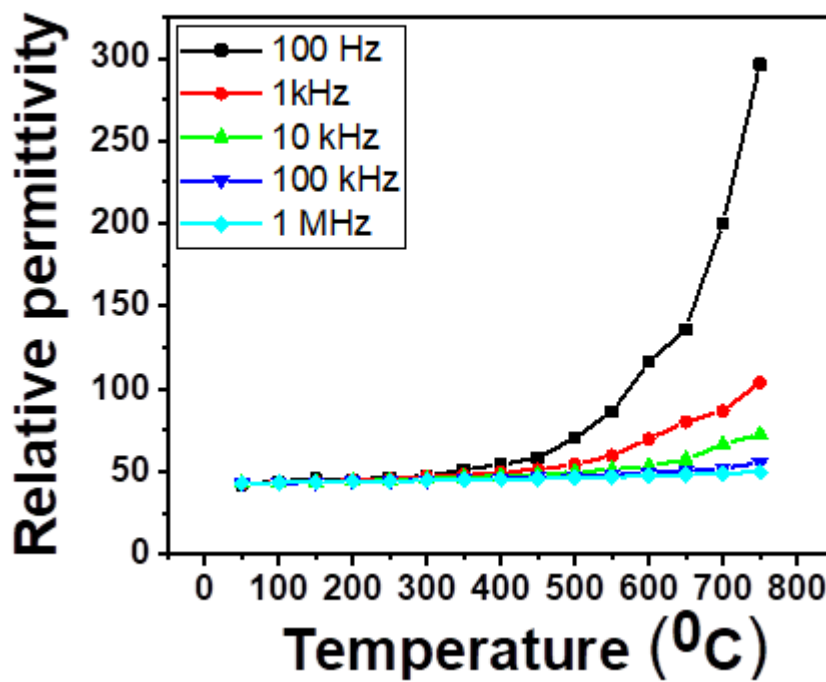Fig4.13: shows Pt deposited pellet connected with Pt wires.

Fig4.14: Shows variation of relative permittivity with temperature and frequency
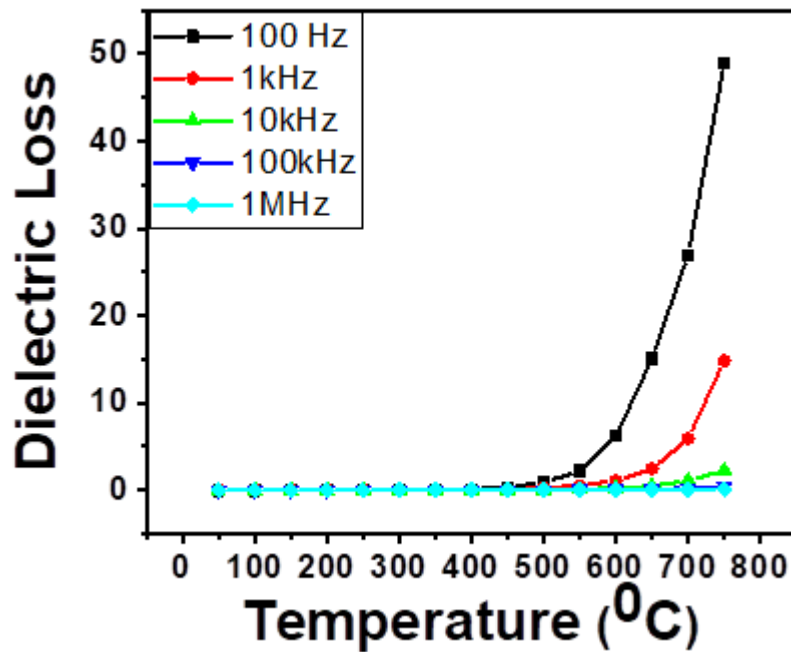
Fig4.15: Shows variation of dielectric loss with temperature and frequency

Dielectric constant decreases with increase in frequency. This decrease is due to the reduction of space charge polarization. With increasing frequency of the electric field the mechanism of polarization such as space charge, dipolar and ionic start lagging behind the field as they cannot follow the high frequency at which field is changing. At low frequency dielectric constant increases due to the presence of space charge polarization effect at the grain boundaries which creates potential barrier. Then accumulation of charge at the grain boundary occurs, which leads high value of dielectric constant.

With increasing temperature dielectric constant increases that follows the Curie – Weiss law [1]

$$\varepsilon = \frac{C}{T - T_0} \qquad (4.11)$$

Electronic and ionic polarizations are independent of temperature but with increasing temperature dipolar polarization decreases and space charge polarization significantly increases. Dielectric constant will increase up to curie temperature of the material with increasing temperature and after that it will decrease, which indicates the ferroelectric to paraelectric phase transition.

Variation of dielectric constant and dielectric loss are similar w.r.t temperature and frequency. With increasing frequency polarization contributions decreases. So dielectric loss also decreases. At low frequency high dielectric loss due to the effect of high resistive grain boundaries. With increasing temperature dielectric loss at a given frequency increases as mobility of the charge carrier increases which increases polarization. High dielectric loss at high temperature because of the charge accumulation at the grain boundaries. At high frequency it shows low dielectric loss which is good for application.

4.8 Pyrocurrent measurement:

Pyrocurrent measurements are considered as the direct evidence of pyroelectric phenomena. As NTO is ferroelectric material, it also exhibits pyroelectric property. In pyroelectric material there is change in spontaneous polarization w.r.t change in temperature. Basically voltage developed and the corresponding current is called pyrocurrent. When the material is heated or cooled, crystal lattice expands or shrinks respectively. So dipole moments also increase or decrease accordingly which polarization changes.

In this experiment, on both sides of NTO pellet platinum is deposited by e-beam deposition technique as electrode material and platinum wires are connected by silver paste. First sample is poled at 200 V for 5 hours and then short circuit the sample for 10 hours to discharge completely. After that Platinum wires are connected to the Source Meter Unit (SMU model No: Keithley 2401) and sample is kept inside furnace. Applied voltage is set to zero and temperature ramping is programed in between 600°C to 500°C. Data is taken current vs time. Initially from 0°C to 600°C heating rate is 10°C/min and after that temperature ramping rate is 5°C/min. Zero current measurement is also done keeping the two adapters in air without applied voltage.
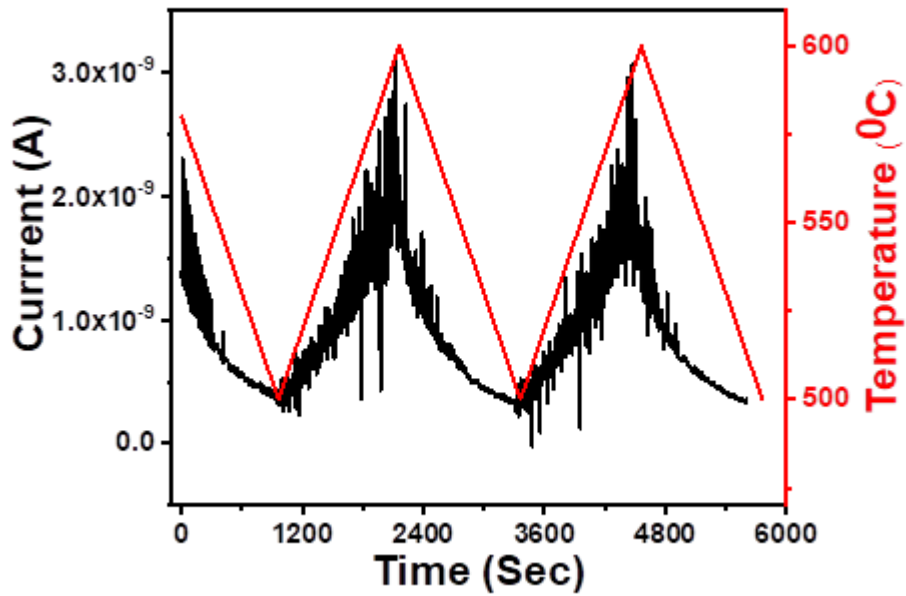
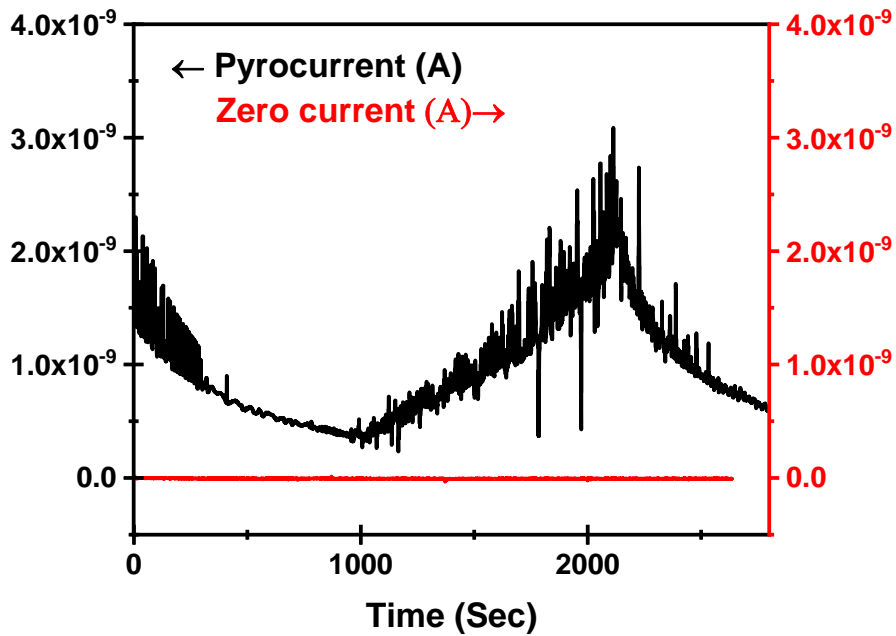Fig4.16: shows variation of pyrocurrent w.r.t temperature ramping

Fig4.17: Comparison between pyrocurrent and thermal noise

According to the graph, pyrocurrent in the order of nano Ampere and zero current in the order of pico Ampere ($\sim 5 - 7\,pA$). Pyrocurrent varies with temperature exponentially. As temperature increases pyrocurrent increases exponentially and as

46

temperature decreases pyrocurrent also decreases exponentially according to the equation:

$$I_p = Ap\frac{dT}{dt} \qquad (4.12)$$

Where, I_p = Pyrocurrent

A = Area of the electrode

p = Pyrocofficient

$\frac{dT}{dt}$ = Rate of change of temperature

So, pyrocurent is proportional to the rate of change of temperature.

$$I_p \; \alpha \; \frac{dT}{dt} \qquad (4.13)$$

That's why according to temperature ramping pyrocurrent increases or decreases exponentially:

$$I = \; I_0 e^{-\frac{t}{\tau}} \qquad (4.14)$$

By taking log on both side graph will be linear and slope will be reciprocal of time constant (τ) which is basically time required for response to decay 37% or to increase 63% of its initial value. For each cycle of ramping slope will be nearly similar. From linear fitting it is clearly seen that slops are similar for all cycle of ramping and it is equal to 0.00148 X 10^{-6} which is a good agreement.

Pyroelectric coefficient calculation:

Pellet dimension:

Thickness = 1.62 mm

Diameter = 8.83 mm

Area = A = πr^2 = 6.12 $\times$ 10^{-5} m^2

Pyroelectric coefficient,

$$p = \; \frac{I}{A\frac{dT}{dt}} = \frac{10^{-9} \times 60}{6.12 \times 10^{-5} \times 278}$$

$$= 3.52 \; \mu C/m^2 K$$

According to temperature ramping data are separated and for each ramping linear fitting is done by origin software. For linear fitting data plotted Ln(I) vs time.
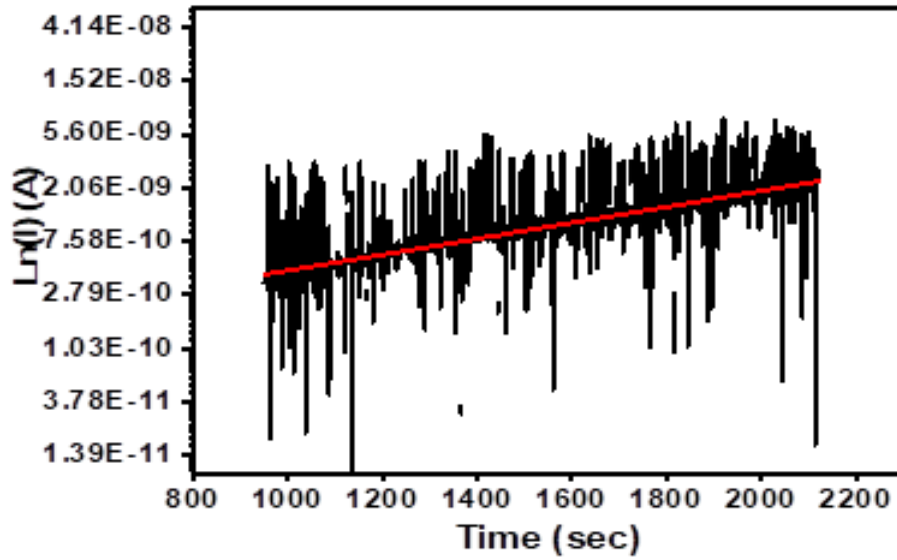

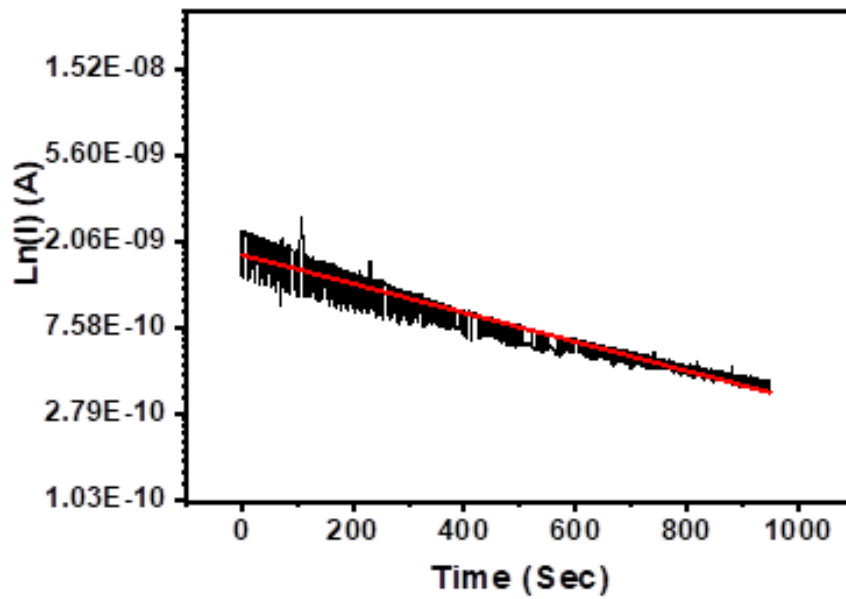Fig.4.18: Shows linear fitting for temperature ramping from 600-500 ˚ C
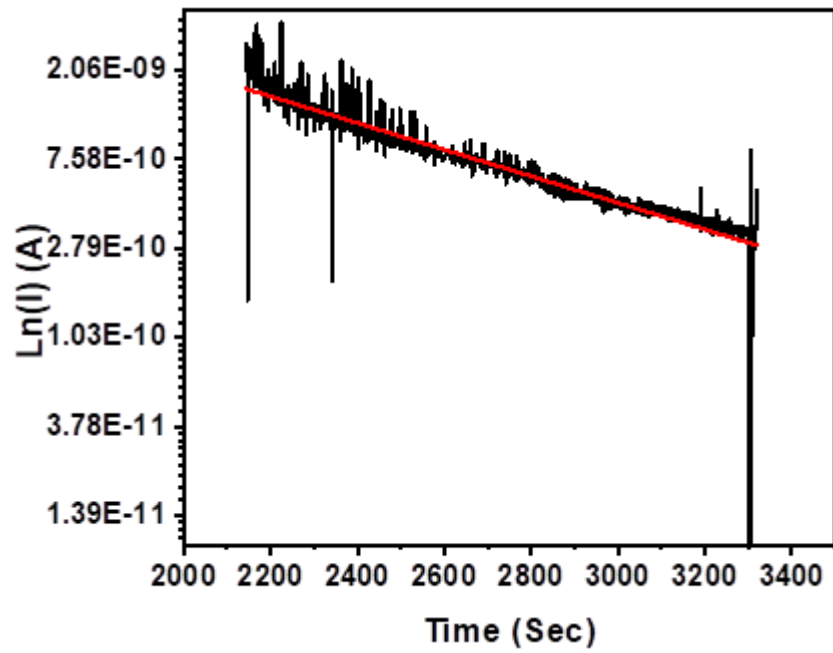

Fig4.19: Shows linear fitting from 500 to 600 ˚ C

48

Fig4.20: Shows linear fitting from 600 to 500 ˚C
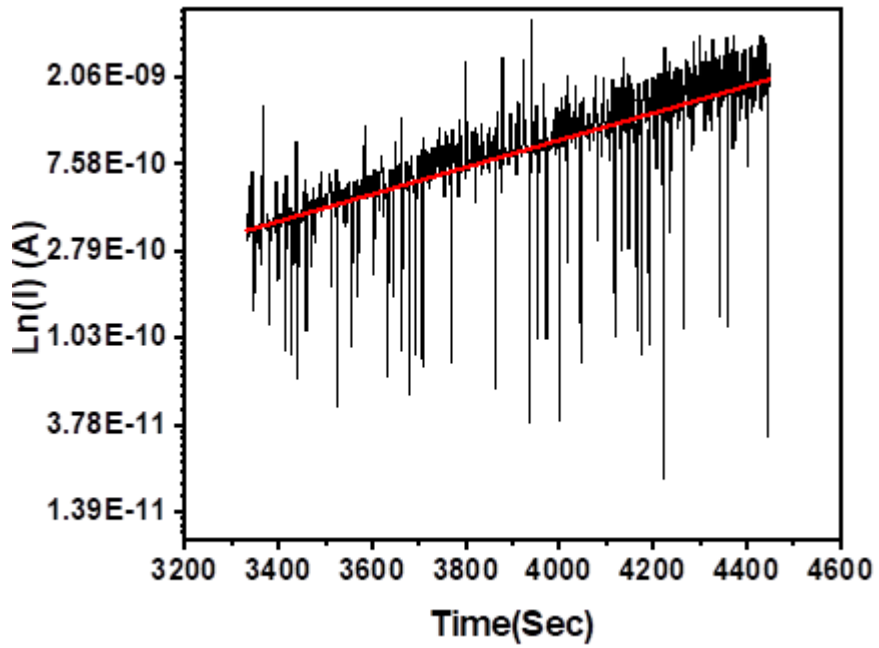
Fig4.21: Shows linear fitting from 500 to 600 ˚C
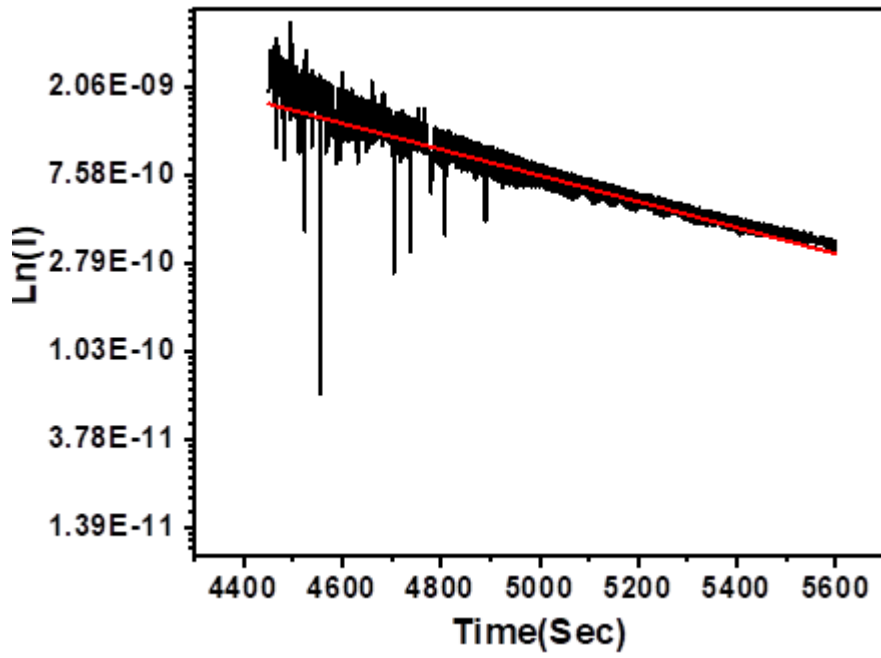
Fig4.22: Shows linear fitting from 600 to 500 ˚C

Ramping of temperature	Slope ($\times \mathbf{10^{-6}}$)
600˚ C - 500˚ C	-0.00148
500˚ C - 600˚ C	+0.00148
600˚ C - 500˚ C	-0.00149
500˚ C - 600˚ C	+0.00156
600˚ C - 500˚ C	-0.00148

Slope is directly proportional to the change in polarization (ΔP), which is almost constant = 0.00148×10^{-6}. This shows good agreement of experiment.

Chapter 5

5.1 Summary and conclusions:

In this project $Nd_2Ti_2O_7$ (Neodymium Titanate) was prepared by solid state reaction route. Stoichiometric mixture of Nd_2O_3 and TiO_2 was ground in mortar and pestle for 4 hours. Then calcination of powder is done with $1250°C$ for 4 hours. Phase purity is observed by X-ray diffraction of powder sample. After ball milling at 200 rpm the powder sample is mixed with PVA binder and pressed to make pellet. Pellets were sintered at $1400°C$ for 5 hours for densification. SEM image of pellet shows how particles are densely packed. EDS analysis shows there is no loss of any element during sintering.

Reitveld refinement of XRD data is done with Fullprof software and confirms the phase, crystal structure, space group and lattice parameters. Unit cell images are created by Vesta software.

Dielectric properties study was carried out with the dense sintered pellet. On both sides of pellet silver paste painted as electrode material and copper wires are connected. Sample kept in furnace and wires are connected to the impedance analyzer adapters. Measurement is done while cooling from $300°C$ within frequency range 50 Hz to 1 MHz. This experiment shows how dielectric constant and dielectric loss varies with temperature. High temperature dielectric study up to $750°C$ is done by depositing platinum on both sides of pellet as electrode material by e-beam deposition and platinum wires are connected using silver paste. Sample were heated inside the furnace and the platinum wires were connected to the impedance analyzer instrument. Data taken from $750°C$ to $50°C$ within frequency range 100 Hz to 1 MHz.

For evidence of pyroelectricity pyro current is measured w.r.t temperature ramping between $600°C$ to $500°C$. On both sides of pellet silver paste painted and platinum wires are connected. Sample kept inside furnace and wires are connected to source meter unit. Current vs time data was taken during temperature ramping between $600°C$ to $500°C$. Graph shows with ramping of temperature current is also exponentially increases or decreases which is nothing but pyrocurrent. Pyrocurrent is measured in the order of nano Ampere and zero current is in the order of pico Ampere. So the material is suitable for temperature sensing application.

5.2 Future work:

➢ Study of structural stability of ferroelectric $Nd_2Ti_2O_7$ thin films deposited on Si and SiC substrate.

➢ Study of high temperature (>1000˚ C) electrical properties of ferroelectric $Nd_2Ti_2O_7$ thin film.

References:

[1] Zhipeng Gao1,2, Chengjia Lu1, Yuhang Wang1, Sinuo Yang3, Yuying Yu1 & Hongliang He1. Super Stable Ferroelectrics with High Curie Point.Scientific Reports 6:24139 (2016)

[2] G. Winfield , F. Azough & R. Freer (1992) DiP224: Neodymium titanate (Nd2Ti2O7)ceramics, Ferroelectrics, 133:1, 181-186

 [3] Nobuo Ishizawa,a* Keisuke Ninomiya,a Terutoshi Sakakurab and Jun Wang. Redetermination of Nd2Ti2O7: a noncentrosymmetric structure with perovskite-type slabs. Acta Cryst. (2013). E69, i19

[4] Ferroelectric, Electrooptic and Piezoelectric properties of Nd2Ti2O7 single crystal.Kimura, Masakazu; Nanamatsu, Satoshi; Kawamura, Tsutomu; Matsush.Japanese Journal of Applied Physics Volume 13 issue 9 1974

[5] K. SCHEUNEMANN and Hk. MOLLER-BUSCHBAUM. ZUR KRISTALLSTRUKTUR VON Nd2Ti2O7.J. inorg, nueL Chem.. 1975, Vol. 37, pp. 2261-2263

[6] Valasek, J. (1921). Piezo-electric and allied phenomena in rochelle salt. Phys. Rev., 17, 475

[7] Sharma, Sumeet Chauhan, Vishal Yadav, C.S. 2018/01/01 A theoretical model for the electromagnetic radiation emission from ferroelectric ceramics VL - 14 10.1016/j.mtcomm.2018.01.002 Materials Today Communications

[8] Nayak, Suryakanta and Sahoo, Banalata and Chaki, Tapan Kumar and Khastgir, Dipak","Facile preparation of uniform barium titanate (BaTiO3) multipods with high permittivity: impedance and temperature dependent dielectric behavior",Journal RSC Adv 2014 volume doi10.1039/C3RA44815K

[9] Matt Dawber's Group, artificially layered ferroelectric oxides, department of physics and astronomy, Stony Brook University

[10] Mishra, Suvrajyoti Unnikrishnan, Lakshmi Kumar Nayak, Sanjay Mohanty, Smita 2018/11/01 Advances in Piezoelectric Polymer Composites for Energy Harvesting Applications: A Systematic Review 10.1002/mame.201800463 Macromolecular Materials and Engineering

[11] Pinin, Own work Perovskite structure of PZT 5 August 2010

[12] Pyroelectric effect: primary and secondary pyroelectric effectpdf

[13] Aboalbiss Own work Bragg's law14 November 2009

[14]The-k-l-m-principle-quantum-number-war-report-on-karl-marx-atomic-class-warfare-school-class-shootings-the-hierarchy-problem-atomic-anthropology-war

[15] W. Cao, synthesis of Nanomaterials by High Energy Ball Milling Skyspring Nanomaterials, Inc.

[16] Spectrolab systems

[17] B.J.Inkson 2 - Scanning electron microscopy (SEM) and transmission electron microscopy (TEM) for materials characterization

[18] Scanning electron microscopy- nanoscience

[19] Ahmadi, Shideh Asim, Nilofar Alghoul, Mohammad Y. Hammadi, F Saeedfar, Kasra Ludin, Norasikin H. Zaidi, Saleem Sopian, Kamaruzzaman 2014/02/09 The Role of Physical Techniques on the Preparation of Photoanodes for Dye Sensitized Solar Cells Volume 2014 10.1155/2014/198734 International Journal of Photoenergy

[20] Parallel plate capacitor, hyper physics concepts

[21] Zulkifli Ahmad Polymer Dielectric Materials October 201210.5772/50638 pub.1011046011

[22] Kisi, Erich - Application of neutron powder diffraction

[23] The Rietveld method – Edited by R. A. Young

[24] Fundamentals of Rietveld Refinement XRD Simulation 2011.pdf

[25] Introduction to Rietveld refinements Luca Lutterotti Department of Materials Engineering and Industrial Technologies University of Trento - Italy

[26] Elements of X-ray diffraction – B.D. Cullity and S.R. Stock